

# Neptune: Advanced ML Operator Fusion for Locality and Parallelism on GPUs

Yifan Zhao<sup>1</sup>, Egan Johnson<sup>1</sup>, Prasanth Chatarasi<sup>2</sup>, Vikram Adve<sup>1</sup>, Sasa Misailovic<sup>1</sup>

<sup>1</sup> University of Illinois Urbana-Champaign <sup>2</sup> IBM Research

## Abstract

Operator fusion has become a key optimization for deep learning, which combines multiple deep learning operators to improve data reuse and reduce global memory transfers. However, existing tensor compilers struggle to fuse complex reduction computations involving loop-carried dependencies, such as attention mechanisms.

The paper introduces Neptune, a tensor compiler for advanced operator fusion for sequences of reduction operators. Neptune presents a new approach for advanced operator fusion, which intentionally breaks some existing dependencies and compensates by constructing algebraic correction expressions that allow the kernel to produce the correct result.

On ten attention-based benchmarks, Neptune, starting from simple attention code and a high-level scheduling template, outperforms existing compilers like Triton, TVM, and FlexAttention, including Triton-based implementations of FlashAttention. Across four different GPU architectures from NVIDIA and AMD, Neptune-generated kernels have average speedup of 1.35x over the next best alternative, demonstrating its effectiveness for deep learning workloads.

## 1 Introduction

Finding high-performance optimizations for modern deep learning models is essential for low-latency and low-cost model deployment. The optimizations translate the high-level model architecture, in the form of a sequence of operators, into a sequence of GPU instructions (“kernels”) that maximize performance and minimize resource usage. Historically, a common strategy is to manually identify the most promising sequences of operators and translate them to a custom hand-optimized kernel [1, 30]. The diversity of DNN architectures and GPU platforms (e.g., PyTorch had over 2000 operators [8]), however, makes this approach non-manageable.

Tensor compilers are emerging as a promising alternative to automatically generate DNN kernels. Compilers that find optimized kernels from a sequence of high-level operators fall into two main approaches: (1) *Schedule-based optimizers*, such as Halide [31] and TVM [6], operate on loop-based programs. They provide composable and flexible primitives for applying a rich set of program transformations, e.g., for loop nests. (2) *Tile-based optimizers*, such as Triton [36] and Pallas [3], operate on tile-based programs, in which *tiles* (fixed-shape multi-dimensional subarrays) are first-class objects. They excel at automatically managing tile data layout/movement and hardware-specific execution.

Operator fusion has emerged as one of the most important compiler transformations that combines multiple operators to obtain high-performance kernels with improved data reuse and reduced global memory transfers. Despite significant progress in recent years, computations with complex loop-carried data dependencies are difficult for tensor compilers to optimize. One prominent example is the attention computation, which is a sequence of four operations: matrix multiplication (matmul), element-wise division, softmax, and another matmul. Three of the four operations are reductions. Because compilers cannot fuse those loop nests, developers resort to manually developed fused kernels, such as FlashAttention [13, 14] and FlashDecoding [15].

We identify two key concerns that prevent existing tensor compilers from achieving fast fused DNN kernels:

- Complex data dependencies prevent compilers from applying operator fusion in cases where fusion would benefit performance. Classical fusion of multiple operations or loop nests cannot be applied because of fusion-preventing dependencies. Alternatively, breaking or reordering some of those dependencies can provide more opportunities, but reasoning about these transformations is difficult for today’s compilers. For instance, reduction loops present in FlashAttention have many loop-carried dependencies that are difficult to reason about.
- Each of the two major tensor optimization approaches is insufficient to find high-performance optimizations alone. Schedule-based optimizers operate in intractable search spaces spanned by sequences of many fine-grained transformations and analyses. While tile optimizers leverage its simpler programming model that captures regular tile computations and a simpler search space, “global” optimizations – such as operator fusion – are presently pushed back to developers. Interactions between schedule and tile optimization pipelines have been virtually non-existent. For instance, to benefit from both TVM’s operator fusion and Triton’s tile optimizations, a developer needs to apply TVM to the operator and manually translate the optimized TVM program into a Triton program.

**Our Work:** We present Neptune, a novel tensor (kernel) compiler that uses advanced operator fusion to generate efficient GPU kernels. Neptune’s kernels fuse multiple reduction operators with complex data dependencies that are beyond the reach of existing popular tensor compilers such as TVM [6],

Triton [36], and OpenXLA [29]. Towards that goal, Neptune makes two key technical innovations:

- We present a paradigm for advanced operator fusion with sequences of reduction operators. It solves the issue of complex data dependencies when fusing reduction operators by 1) intentionally breaking some of those dependencies (“naive fusion”) and 2) constructing algebraic correction expressions (“repair terms”) that allow the kernel to produce the correct result by the end of its execution. By adding a small amount of computation and cache memory, the transformation reduces global memory transfers and improves data reuse.

We present two instantiations of this paradigm: Rolling Update Fusion and Split-K Fusion. Both transformations are particularly suited for optimizing attention-like operators. Rolling Update Fusion is well-suited for attention in prefill mode, such as FlashAttention. Split-K Fusion is well-suited for decoding attention, such as FlashDecoding. Both algorithms operate as transformations in schedule-based compilers and can be combined with other loop and algebraic transformations.

- We present a pipeline that integrates scheduling and tile-based optimizations. It separates low-level optimizations, which the tile optimizer handles, and high-level optimizations as primitives in its scheduling language, keeping scheduling concise and simplifying the search space. Scheduling applies to a loop-scalar IR that consists of loop nests and scalar expressions, which is well-suited for expression-manipulating transformations such as rolling update. After scheduling, Neptune’s translation engine detects sections of regular tile computation in the program via pattern matching, and offloads them to its tile optimizer.

These two innovations represent key building blocks for supporting – *natively within a compiler* – advanced high-performance attention-algorithm optimizations, similar to FlashAttention and FlashDecoding. Neptune takes as input a sequence of operators to optimize (e.g., a “vanilla” attention), typical input shapes (e.g., sequence lengths), and a schedule template for high-level optimizations (similar to Halide’s/TVM’s). Neptune identifies the computations that can be fused and generates optimized GPU kernels.

We evaluate Neptune on 10 different attention-based operators from the literature, on multiple GPU architectures from NVIDIA and AMD and different sequence lengths. Our results show that Neptune-generated kernels have lower latency than those of other compiler-based frameworks, Triton [36], TVM [6], FlexAttention [17], and Mirage [39], including Triton-based implementations of FlashAttention. Out of 320 optimized configurations (combinations of operators, sequence lengths, and GPUs), Neptune generates the lowest-latency kernel in 284 cases, with speedup over the next best, already highly optimized alternative of 1.35× (geomean). Further, in 101 out of 256 configurations, Neptune improves over

the state-of-the-art kernels provided by CUTLASS [27] based library implementations.

**Contributions:** The paper makes several contributions:

- We present Neptune, a tensor compiler that supports advanced loop fusion algorithms for reduction operators, while leveraging the advantages of both schedule-based and tile-based GPU optimization of tensor programs.
- We present a novel optimization approach for operator fusion that satisfies data dependency by recomputation and automatically derives required algebraic repairs. Two instances, Rolling Update Fusion and Split-K Fusion, are particularly suited for optimizing attention-like operators.
- We present translation from scheduled loop programs to tile programs that a standard tile optimizer can efficiently optimize, which frees schedules from low-level optimizations so schedules can focus on high-level optimizations.
- We implement Neptune on top of the Apache TVM schedule tensor compiler and the Triton tile tensor compiler. Neptune’s optimization approach is general and can be implemented over other similar tensor compilers for ML.
- Our thorough evaluation of Neptune shows that Neptune produces kernels that are faster than existing compilers by 1.35× (geomean), on a diverse set of attention variants and four GPU architectures from Nvidia and AMD.

Neptune is available at <https://github.com/uiuc-arc/neptune>.

## 2 Motivation

Figure 1 shows an example of the reduction fusion problem, where data dependencies make loop fusion challenging. The code in Figure 1a runs on a 2-by-4 matrix  $\text{inp}$  and has three loop nests: a row-wise max  $\text{s\_max}$ , an element-wise exponential  $\text{s\_exp}$ , and a row-wise sum  $\text{s\_sum}$ . Figure 1d shows a concrete execution of the program, where blue arrows mark data dependencies. We denote  $x_{ij} := \text{inp}[i, j]$ ,  $p_{ij} := \text{xexp}[i, j]$ . We denote  $s_i^{(j)}$  as the value of  $\text{xsum}[i]$  at iteration  $j$ , and  $m_i^{(j)}$  as the value of  $\text{xmax}[i]$  at iteration  $j$ . The final result of this program is  $s_i^{(3)}$ .

Fusing  $\text{s\_exp}$  into the reduce loop nest  $\text{s\_max}$  is an example of reduction fusion that today’s loop fusion is not capable of. Figure 1b shows the incorrect program that current loop fusion would produce, if we naively fuse  $\text{s\_exp}$  and  $\text{s\_sum}$  into  $\text{s\_max}$ , by disregarding loop-carried dependencies between the  $\text{s\_max}$  and  $\text{s\_exp}$ . Figure 1e shows its execution on a concrete  $\text{inp}$  matrix, illustrating why the naive fusion is incorrect: fusing  $\text{s\_exp}$  under  $\text{loop\_j}$  changes some  $\text{s\_exp}$  iterations to read from  $\text{xmax}$  too early. The brown arrows mark these incorrect data dependencies. For example, in the first iteration,  $p_{i0}$  reads from  $m_i^{(0)}$  at the same iteration, instead of  $m_i^{(3)}$  computed after 4 iterations. Thus, the result of  $p_{ij}$  is incorrect and propagates to the final result  $s_i^{(3)}$ . In practice, tensor compilers would reject this incorrect fusion.

However, correct reduction fusion is possible if we *update the compute expressions* in addition to changing the loop

```

# s_max:
for i in range(2):
    for j in range(4): # loop_j
        xmax[i] = max(xmax[i], inp[i, j])
# s_exp:
for i, j in grid(2, 4):
    xexp[i, j] = exp(
        inp[i, j] - xmax[i])
# s_sum:
for i, j in grid(2, 4):
    xsum[i] += xexp[i, j]

```

(a) The original program, consisting of 3 loop nests `s_max`, `s_exp`, and `s_sum`.

```

for i in range(2):
    for j in range(4): # loop_j
        # s_max:
        xmax[i] = max(xmax[i], inp[i, j])
        # s_exp:
        xexp[i, j] = exp(
            inp[i, j] - xmax[i])
        # s_sum:
        xsum[i] += xexp[i, j]

```

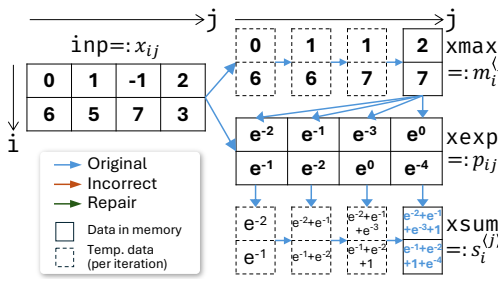
(b) An incorrect naively fused version of Figure 1a. `s_exp` and `s_sum` are fused under `loop_j` without considering the data dependencies.

```

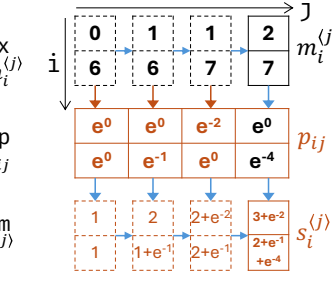
for i in range(2):
    xmax_0[i] = -inf
    for j in range(4): # loop_j
        # s_max:
        xmax_1[i] = max(xmax_0[i], inp[i, j])
        # s_sum:
        xsum[i] = (
            exp(xmax_0[i] - xmax_1[i]) * xsum[i]
            + exp(inp[i, j] - xmax_1[i]))
        xmax_0[i] = xmax_1[i]

```

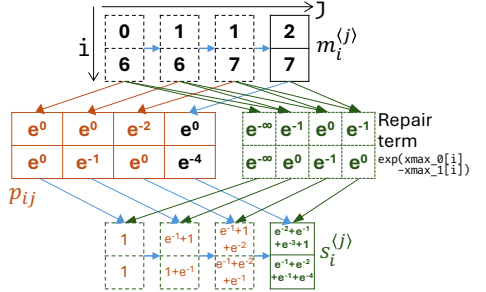
(c) Correct fusion of Figure 1a, which also inlines `s_exp` and edits the compute expressions of `s_sum` in addition to Figure 1b.



(d) Materialized example of Figure 1a. Data dependencies are shown in blue.



(e) Materialized example of Figure 1b; `inp` is omitted; incorrect results and dependencies are shown in blue.



(f) Materialized example of the correctly fused Figure 1c. Values of the repair term and the repaired xsum are shown in green. Note,  $s_i^{(3)} = s_i^{(3)}$

**Figure 1.** An example program requiring reduction fusion, incorrect result using naive loop fusion, and a correctly fused program, shown on the first row. The second row (“materialized example”) shows the values of each matrix in the programs when applied to a concrete `inp` matrix. `xmax` and `xsum` are each shown four times since their values vary over `j` iterations.

structure. We can find new expressions for `s_exp` and `s_sum` that not only compute results for the current iteration, but also *repair* results from the previous iteration, as we move forward in the reduce dimension `j`. Figure 1c shows the correct fusion result that builds on this idea. This program multiplies a *repair term*  $\exp(xmax_0[i] - xmax_1[i])$  with `xsum[i]`. Figure 1f shows the values of this repair term and the repaired  $s_i^{(j)}$  values. The repaired program is correct because  $s_i^{(3)}$  is equal to  $s_i^{(3)}$ , even though  $s_i^{(j)} \neq s_i^{(j)}$  for  $j < 3$ .

To show how the repair term repairs the `xsum[i]` at every `j` iteration, we write out  $s_i^{(j)}$  for three iterations, as an expression of `xij` and  $m_i^{(j)}$ :

$$\begin{aligned}
s_i^{(0)} &= \exp(x_{i0} - m_i^{(0)}); \\
s_i^{(1)} &= \exp(m_i^{(0)} - m_i^{(1)}) \cdot s_i^{(0)} + \exp(x_{i1} - m_i^{(1)}) \\
&= \exp(m_i^{(0)} - m_i^{(1)}) \cdot \exp(x_{i0} - m_i^{(0)}) + \exp(x_{i1} - m_i^{(1)}) \\
&= \exp(x_{i0} - m_i^{(1)}) + \exp(x_{i1} - m_i^{(1)}) \\
s_i^{(2)} &= \exp(m_i^{(1)} - m_i^{(2)}) \cdot (\exp(x_{i0} - m_i^{(1)}) + \exp(x_{i1} - m_i^{(1)})) \\
&\quad + \exp(x_{i2} - m_i^{(2)}) \\
&= \exp(x_{i0} - m_i^{(2)}) + \exp(x_{i1} - m_i^{(2)}) + \exp(x_{i2} - m_i^{(2)}) \quad (1)
\end{aligned}$$

We observe that the following behavior is key to a working repair term: at each iteration  $j$ , the repair term multiplies with

the previous iteration result  $s_i^{(j-1)}$ , which is an expression of  $m_i^{(j-1)}$ , and replaces all uses of  $m_i^{(j-1)}$  with  $m_i^{(j)}$ , as shown in Equation 1. This repair term is a *tag updater* (considering that  $\langle j \rangle$  is a tag on the array access). We show in Section 4 that Neptune automatically finds this repair term for a large class of programs.

This solution of reduction fusion as shown in Figure 1c adds a small number of instructions to compute the repair term, as the repair term is a short expression calculated once per iteration. It also adds some memory overhead to keep the previous iteration of reductions (i.e. `xmax_0` and `xmax_1`), in GPU registers or shared memory. This memory overhead is low as the reduction output arrays are small compared to other arrays in the program, such as `xexp` and `inp`. These overheads trade off with the benefit of reduced memory pressure, which is often profitable on GPUs.

### 3 System Overview

Figure 2 summarizes the main components of Neptune and sections in this paper where we describe them. Neptune takes as input a program written in tensor expression and a template of transformations for the program. Transformation template is a user-provided recipe with a list of high-level optimizations to apply to the program. The compiler optimizes programs using the following steps:

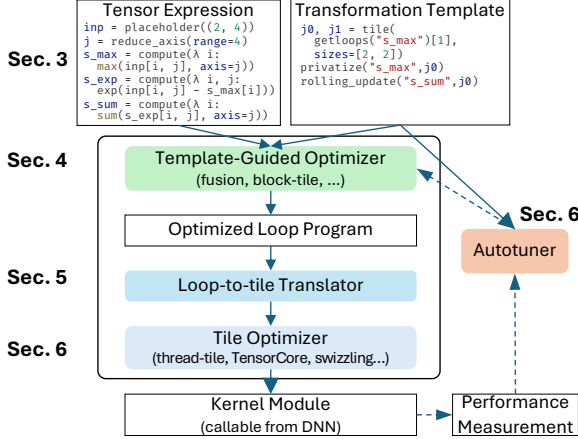


Figure 2. The main components of Neptune.

- The template-guided optimizer automatically applies the transformations in the template to the loop nests in the program. Section 4 presents two novel advanced fusion algorithms that compose with other built-in transformations. At this point, we have a loop-scalar program that has undergone high-level optimizations.
- To facilitate tile optimizations, the loop-to-tile translator automatically identifies tensorizable expressions, which we describe in Section 5. The tile optimizer applies tile-specific transformations on the program (e.g., data movement, tile data layout, and HW-specific execution) and produces an executable kernel.
- Neptune has an autotuner that tunes parameters in the transformation template, which we describe in Section 6.

**Input: Tensor Expression.** Neptune provides a compact expression language for the user to define the computation of the program. Tensor expressions translate straightforwardly into Neptune’s loop-scalar IR. Figure 2 (top left) shows tensor expressions that produce the loop program in Figure 1a. Tensor expressions are written in TVM expression language here; JAX’s jaxpr language could be used instead in principle.

**Input: Transformation Template.** A transformation template is a list of transformation steps the user writes to describe how to optimize the program. Each step calls a transformation primitive in Neptune, with parameters that describe where to apply the transformation on the program. The template-guided optimizer applies each step in the template to the program. We describe the optimizer and the transformation primitives available in Section 3. Figure 2 (top right) shows an example template that is applicable to the given tensor expression program.

While transformation templates resemble the scheduling languages used in some tensor compilers, Neptune’s template is concise. In a few lines of code, a user can express all the transformations needed to optimize a complex operator with multiple loop nests. Transformation templates only describe high-level optimizations that benefit from user direction, while Neptune delegates low-level optimizations to its

tile optimizer, without user intervention. An example of tensor expression and schedule for attention is in Appendix A.

**Preliminaries and Notation.** We define notations we will use next; some common notations are in Appendix B. We use a compact notation for loop nests:  $\text{nest}(\mathbf{i}:\mathbf{n})\{s\}$  to represent  $K$  perfectly nested loops with upper bounds  $\mathbf{n} := (n_1, \dots, n_K)$  and body  $s$ .  $\mathbf{i} \in \mathbb{Z}^K$  is an iteration vector of the nest. The iteration domain  $\mathcal{D}^s$  is the set of values  $\mathbf{i}$  can take, given by  $\mathbf{n}$ . We denote the previous iteration of  $\mathbf{i}$  as  $\text{prev}(\mathbf{i})$  and the next iteration as  $\text{next}(\mathbf{i})$ .

In a tensor access  $X[\phi(\mathbf{i})]$  in a loop nest (iteration vector  $\mathbf{i}$ ),  $\phi$  is an *affine access function* that projects  $\mathbf{i}$  to tensor indices. In Figure 1b, the tensor store  $\text{xsum}[\mathbf{i}]$  has an access function  $\phi(i, j) = i$ . When a tensor entry is updated multiple times, we add a *tag* on the access to mark which iteration we refer to:  $X[\phi(\mathbf{i})]^{(j)}$  ( $\text{xsum}[\mathbf{i}]^{(j)}$  for example). Tags reflect temporal data dependency on the same tensor entry.

In a reduction, the reducer  $f$  is an associative binary function. We use  $a \mathcal{f} b$  to express  $f(a, b)$ . We define the reduce operator  $\mathcal{R}$  to express the value of a reduction compactly:  $\mathcal{R}(f, 0 \leq j \leq j_0, g(j))$  applies  $f$  to fold over  $g(j)$  from  $j=0$  to  $j_0$  to produce a single value. For instance,  $\mathcal{R}(+, 0 \leq j \leq 2, \text{xexp}[i, j])$  equals  $\text{xexp}[i, 0] + \text{xexp}[i, 1] + \text{xexp}[i, 2]$ .

## 4 Template-Guided Optimizer

The template-guided optimizer translates the input program given as tensor expressions into Neptune’s loop-scalar IR, and applies the transformation primitives in the template to the program. The abstract syntax of this IR is in Appendix E; it is similar to the loop-level IR in many tensor compilers. This level includes standard loop transformations, data layout transformations, and data placement transformations (e.g., caching in shared memory). Neptune also provides novel transformations that permit reduction fusion, described next.

### 4.1 Rolling Update

Rolling update is Neptune’s novel transformation solving the reduction fusion problem described in Section 2. It applies to a reduce loop nest  $L_t$  to be fused and a target loop  $l$  (the *rolling loop*) to fuse  $L_t$  under:  $\text{RollingUpdate}(L_t, l)$ . Rolling update requires that  $L_t$  depends on at least one reduce loop nest, such as  $\text{s\_sum}$  depends on  $\text{s\_max}$  through  $\text{s\_exp}$  in Figure 1a.

Algorithm 1 outlines the full rolling-update algorithm. There are five major steps in rolling update, which we explain in the following paragraphs. When any step fails (such as pattern matching and repair function solving), rolling update returns the original program. A step-by-step example of applying rolling update on Figure 1a is in Appendix C.

**Dataflow Reorganization.** Rolling update performs an analysis on the dataflow graph to find and manipulate predecessors of  $L_t$ . On line 1, `INLINEMAPRETURNREDUCE` finds predecessors of  $L_t$  that are reduce loop nests, as a set  $\mathcal{L}_r$ , called the *reduce predecessors* of  $L_t$ . Then on each path from  $L_t$  that

---

**Algorithm 1:** ROLLINGUPDATE( $L_t, l$ )

---

**Input:**  $L_t$ : the target loop nest to be fused.  
 $L_t$  holds a reference to the entire program.  
**Input:**  $l$ : the loop to fuse  $L_t$  under (“rolling loop”).  
**Output:** The fused loop nest

- 1  $\mathcal{L}_r = \text{INLINEMAPRETURNREDUCE}(L_t);$
- 2 **for**  $L \in \mathcal{L}_r \cup \text{set}(L_t)$  **do**
- 3     $L = \text{NAIVELOOPFUSION}(L, l);$
- 4     $(f, g) = \text{MATCHREDUCEPATTERN}(L_t, \mathcal{L}_r);$
- 5     $h = \text{SOLVEREPAIRFUNC}(g);$
- 6     $\text{VALIDATEHCOMMUTATIVE}(h, f);$
- 7     $M_x = \text{dict}();$
- 8    **for**  $L \in \mathcal{L}_r$  **do**
- 9       $(x_{\text{prev}}, x_{\text{curr}}) = \text{CACHEREDUCEPREVRESULT}(L);$
- 10      $M_x[L] = (x_{\text{prev}}, x_{\text{curr}});$
- 11     $L_t = \text{APPLYREPAIRTERM}(L_t, h, M_x);$
- 12 **return**  $L_t$

---

ends in  $\mathcal{L}_r$  (excluding both ends), rolling update inlines all the loop nests. These inlined loop nests are map loop nests and predecessors of  $L_t$ , so their computation eventually accumulates in  $L_t$ . After inlining, all of  $\mathcal{L}_r$  are direct producers of  $L_t$ .

**Loop Transformation.** On lines 2 to 3, rolling update fuses  $L_t$  and each of  $\mathcal{L}_r$  under  $l$  using naive loop fusion, skipping loop nests is already under  $l$ . This step ensures that all loop nests in  $\mathcal{L}_r$  share an outer loop nest with  $L_t$ .  $L_t$  now is a fused loop nest producing incorrect results and needs to be repaired.

**Code Pattern Matching.** Pattern matching gathers important information to prepare for solving the repair function next. On line 4, MATCHREDUCEPATTERN matches the compute statement of  $L_t$  and  $\mathcal{L}_r$  simultaneously. It requires  $L_t$  and each  $L_i \in \mathcal{L}_r (i \in \{1, \dots, |\mathcal{L}_r|\})$  to be a reduction.

The structure of  $L_t$  is critical to expression repair, so we zoom in on it.  $L_t$  is already a reduce loop nest:  $L_t = \text{rnest}(\mathbf{i}: \mathbf{n}, j: \mathbf{m})\{s_t\}$ . For the body  $s_t$ , we further capture any computation on the right of the reducer  $f$  into a function  $g: \mathcal{X} \times \mathcal{X} \rightarrow \mathcal{X}$ , to arrive at the specific pattern

$$X_t[\phi_t(\mathbf{i})] = X_t[\phi_t(\mathbf{i})] \circledcirc g(X_r[\phi_r(\mathbf{i})], C[\phi_c(\mathbf{i}, j)]) \quad (2)$$

$X_t$  is the output of  $L_t$ ,  $X_r$  is the output of the reduce predecessor of  $L_t$  (which is  $L_r$ ), and  $C$  is a constant input (such as program input).  $j$  does not index  $X_t$  or  $X_r$  because  $j$  is the reduce loops for both  $L_t$  and  $L_r$ .

Eq. 2 assumes one reduce predecessor  $L_r$  and one constant input  $C$  for simplicity. If there are multiple reduce predecessors and constant inputs, they are added to the arguments of  $g$  without affecting the structure of the pattern.

**Finding the Repair Function.** Rolling update now solves for a *repair function* that it will use to repair  $L_t$  and produce a correct program. A correct program is one where the fused  $L_t$  produces the same result as in the original program. The intuition of how the repair function works comes from Eq. 1 in the motivating example, where we have demonstrated the

*tag-updating* behavior of the repair term. We now generalize from the example and formalize this behavior.

In Eq. 1, the repair term is computed from  $m_i$  of the previous and current iterations, and multiplies with  $s_i^{(j-1)}$  to tag-update it. Generalizing from the example, we see a repair function  $h(t, r, r')$  that accepts three arguments: the value of  $X_t[\phi_t(\mathbf{i})]$  to be tag-updated, and the value of  $X_r[\phi_r(\mathbf{i})]$  in the previous (as  $r$ ) and current (as  $r'$ ) iterations.

Since tag-update involves modifying the tags on  $X_r$  inside the expression of  $X_t$ , it helps to have the explicit expression of  $X_t$  before we formally describe tag-updating. In Eq. 1, every  $s_i^{(j)}$  is an expression  $m_i^{(j)}$  with the same tag  $j$ . Taking that to our general notation, we get the explicit form of  $X_t$ :

$$X_t[\phi_t(\mathbf{i})]^{(j)} = \mathcal{R}(f, 0 \leq j' \leq j, g(X_r[\phi_r(\mathbf{i})]^{(j)}, C[\phi_c(\mathbf{i}, j)])) \quad (3)$$

This expression (with  $X_t[\phi_t(\mathbf{i})]^{(j)}$  in color) generalizes Eq. 1. It is the result we *want* to compute, not what the current program computes. It leads us to the definition of tag-updating:

**Definition 4.1.** A function  $h$  is *tag-updating* if it satisfies

$$\begin{aligned} \forall j \in \mathcal{D}^s. h\left(\mathcal{R}(f, 0 \leq j' \leq j, g(X_r[\phi_r(\mathbf{i})]^{(j)}, C[\phi_c(\mathbf{i}, j)]))\right. \\ \left. X_r[\phi_r(\mathbf{i})]^{(j)}, X_r[\phi_r(\mathbf{i})]^{(\text{next}(j))}\right) \\ = \mathcal{R}\left(f, 0 \leq j' \leq j, g(X_r[\phi_r(\mathbf{i})]^{(\text{next}(j))}, C[\phi_c(\mathbf{i}, j)])\right) \end{aligned}$$

This definition shows that  $h$  tag-updates through a reduce expression that has repeated uses of  $f$  and  $g$ . We propose the following sufficient conditions that are simpler:

**Theorem 4.2.** If a function  $h$  satisfies the following two conditions, then it is tag-updating:

$$h(g(r, c), r, r') = g(r', c) \quad \forall r, r', c \in \mathcal{X} \quad (4)$$

$$h(x \circledcirc y, r, r') = h(x, r, r') \circledcirc h(y, r, r') \quad \forall x, y, r, r' \in \mathcal{X} \quad (5)$$

Namely,  $h$  replaces the  $r$  argument of  $g$ , and  $h$  commutes with the reducer  $f$ . On algorithm line 5, rolling update solves Eq. 4 to find  $h$ , and then proves Eq. 5 for this  $h$  on line 6. We further have the following result on how to solve Eq. 4:

**Theorem 4.3.** If  $y = g(x, c)$  is invertible in the second argument  $c$  to yield  $c = g_c^{-1}(x, y)$ , then Eq. 4 has a solution:

$$h(t, r, r') = g(r', g_c^{-1}(r, t)) \quad (6)$$

Theorem 4.3 allows us to find  $h$  explicitly using symbolic solvers [23]. An intuitive explanation of Eq. 6 is that the  $g_c^{-1}$  term recovers the constant input read from the  $C$  array, before we apply  $g$  with the updated  $r'$  to get the new  $g$  output.

**Applying the Repair Function.** Since we have found an  $h$  that tag-updates  $X_t$ , we apply it to the  $X_t$  of the previous iteration, i.e., we rewrite Eq. 2 into

$$\begin{aligned} X_t[\phi_t(\mathbf{i})] = h\left(X_t[\phi_t(\mathbf{i})], X_r[\phi_r(\mathbf{i})]^{(\text{prev}(j))}, X_r[\phi_r(\mathbf{i})]^{(j)}\right) \\ \circledcirc g(X_r[\phi_r(\mathbf{i})], C[\phi_c(\mathbf{i}, j)]) \end{aligned} \quad (7)$$

This rewrite displays an issue:  $h$  requires  $X_r$  from two iterations, but a reduce loop nest only has the output of the current iteration. The algorithm lines 8-10 fix this issue by caching the result of the last iteration. It transforms each  $L_i \in \mathcal{L}_r$  to retain its previous result temporarily until  $h$  uses it. Finally, line 11 applies the rewrite above and concludes the rolling update algorithm.

**Correctness of the Repaired Program.** We list the two proof goals that show the repaired program is correct: (1) The rewrite result in Eq. 7, which defines  $X_t$  in recurrent form, matches the explicit form Eq. 3. (2)  $X_t$  in Eq. 7 matches the  $X_t$  of the original program, per our definition of program correctness. Theorems 4.4 and 4.5 capture the two proof goals respectively. We prove these theorems in the appendix Section D.

**Theorem 4.4.** *If  $h$  tag-updates  $X_t$ , then  $X_t$  in the recurrent Eq. 7 that uses  $h$  equals  $X_t$  in the explicit Eq. 3.*

**Theorem 4.5** (Correctness of the Repaired Program). *The explicit Eq. 3 produces the same  $X_t$  value as the original program at the end of the  $L_t$  loop nest in both programs.*

Theorems 4.2 – 4.5 together form the basis of rolling update correctness. The proofs of these theorems use the associative property of the reducer  $f$ , which is true for real ( $\mathbb{R}$ ) inputs. In practice, rolling update applies to programs over floating-point inputs, for which  $f$  is not strictly associative. We empirically check the numerical accuracy of the transformed program and find it to be acceptable.

**Tradeoffs of Rolling Update.** Rolling update implements reduction fusion. It extends loop fusion to a mix of elementwise and reduction operations, bringing the benefits of loop fusion: reducing memory pressure and peak memory usage. On the other hand, rolling update adds extra computation to the target loop nest  $L_t$  due to the repair term  $h$ . Moreover, since the new program maintains the result of last and current iterations, the rolling loop  $l$  becomes harder to parallelize due to more complex data flow. We describe a another fusion approach in Section 4.3 that alleviates the second issue.

## 4.2 Reduction Privatization

Neptune provides a variant of *privatization*, a standard program transformation in the compiler literature. Neptune provides privatization as a scheduling primitive that applies to a reduce loop  $l$  in a loop nest  $L$  and requires a tile size  $k$ :  $\text{PrivatizeReduce}(L_t, l, k)$ . It splits  $l$  into an outer loop of size  $k$  and an inner loop, thereby decomposing the reduce loop nest  $L$  into a “local” and a “global” loop nest. The local loop nest executes reduction on a slice of input elements, and the global loop nest combines the local results.

Neptune provides naive loop fusion followed by privatization as one transformation primitive:  $\text{FuseAndPrivatize}(L_t, l)$ . Naive loop fusion produces a loop nest structure that privatization exploits, such that the user does not need to provide a loop tile size  $k$ . The next transformation primitive we introduce uses this variant of privatization.

```

for i, j0 in grid(2, 2):
    for j1 in range(2): # s_max_local
        max_l[i, j0] = max(max_l[i, j0], inputs[i, j0 * 2 + j1])
    for j1 in range(2): # s_sum_local
        sum_l[i, j0] += exp(inputs[i, j0 * 2 + j1] - max_l[i, j0])
for i, j0 in grid(2, 2): # s_max_global
    max_g[i] = max(max_g[i], max_l[i, j0])
for i, j0 in grid(2, 2): # s_sum_global
    sum_g[i] += exp(max_l[i, j0] - max_g[i]) * sum_l[i, j0]

```

**Figure 3.** The result of applying split-k update to Figure 1a.

---

## Algorithm 2: SPLITKUPDATE( $L_t, l$ )

---

```

Input:  $L_t$ : the target loop nest to be fused
Input:  $l$ : the target loop to fuse  $L_t$  under
Output: A pair of loop nests:
    the local and global versions of fused  $L_t$ 
1  $\mathcal{L}_r = \text{INLINEMAPRETURNREDUCE}(L_t);$ 
2  $(M^{\text{local}}, M^{\text{global}}) = (\text{dict}(), \text{dict}());$ 
3 for  $L \in \mathcal{L}_r$  do
4    $(L^{\text{local}}, L^{\text{global}}) = \text{FUSEANDPRIVATIZE}(L, l);$ 
5    $(M^{\text{local}}[L], M^{\text{global}}[L]) = (L^{\text{local}}, L^{\text{global}});$ 
6  $L_t = \text{REPLACETENSORREADS}(L_t, M^{\text{local}});$ 
7  $(L_t^{\text{local}}, L_t^{\text{global}}) = \text{FUSEANDPRIVATIZE}(L_t, l);$ 
8  $h = \text{ROLLINGUPDATESOLVEREPAIRFUNC}(L_t^{\text{local}}, \mathcal{L}_r);$ 
9  $L_t^{\text{global}} = \text{SPLITKAPPLYREPAIRTERM}(L_t^{\text{global}}, h, M^{\text{local}});$ 
10 return  $(L_t^{\text{local}}, L_t^{\text{global}});$ 

```

---

## 4.3 Split-K Update

Neptune is capable of another transformation *split-k update*, which also performs reduction fusion. While rolling update makes the rolling loop harder to parallelize, split-k update avoids this issue and aims to maximize parallelism. This transformation is so named because it resembles the split-k strategy in matrix multiplication [9]. Split-k is well-suited for fusing attention-like operators and produces kernels similar to FlashDecoding [15].

Split-k update reuses the steps 1, 3, and 4 of rolling update: dataflow reorganization, code pattern matching, and finding the repair function  $h$ . In split-k update, our insight on how to tag-update reduction results remains the same, but there are key differences in how we apply loop transformations. Figure 3 shows the result of applying split-k update to the example in Figure 1a. Split-k update partitions the program into a local and a global section. The local section consists of parallelizable reductions,  $s_{\text{max\_local}}$  and  $s_{\text{sum\_local}}$ , that accumulate partial results, while global reductions  $s_{\text{max\_global}}$  and  $s_{\text{sum\_global}}$  combine these partial results into the final result. This local-global split is the key of the loop transformation in split-k update.

Algorithm 2 outlines the split-k update algorithm. We explain this algorithm in comparison to rolling update:

- Split-k update applies step 1 of rolling update to get  $\mathcal{L}_r$ .

- On algorithm lines 2 to 5, split-k update uses the fusion + privatization primitive to fuse all reduce predecessors of  $L_t$  under  $l$ , and tracks their local and global loop nests.
- Line 6 replaces tensor reads in  $L_t$  such that it reads from the local nests of the reduce predecessors. Line 7 fuses and privatizes  $L_t$  under  $l$ .
- Line 8 reuses rolling update steps 3 and 4 to find the repair function  $h$  from  $L_t^{\text{local}}$ , which we show as a single line.
- Line 9 applies the repair function  $h$  to the global nest  $L_t^{\text{global}}$ .

**Applying the Repair Function  $h$  (Split-K).** Split-k update does not apply the repair function to the local section, keeping the local section parallelizable. Instead, it repairs the global loop nest  $L_t^{\text{global}}$  to make the final result correct. Another difference from rolling update is that split-k applies the repair function on the right-hand side of the reducer. Both differences show in the example:  $s\_sum\_global$  has the store statement  $\text{sum\_g}[i] = \text{sum\_g}[i] + \underline{\exp(\text{max\_l}[i, j_0] - \text{max\_g}[i])} * \text{sum\_l}[i, j_0]$  where the underlined term is the repair term.

Split-k update applies the repair function with this rewrite:

$$\begin{aligned} X_{t,g}[\phi_{t,g}(i)] &= X_{t,g}[\phi_{t,g}(i)] \text{ (f)} X_{t,l}[\phi_{t,l}(i)] \\ \Rightarrow X_{t,g}[\phi_{t,g}(i)] &= X_{t,g}[\phi_{t,g}(i)] \\ &\quad \text{(f)} h(X_{t,l}[\phi_{t,l}(i)], X_{r,l}[\phi_{r,l}(i)], X_{r,g}[\phi_{r,g}(i)]) \end{aligned} \quad (8)$$

The first line is the body of the global nest  $L_t^{\text{global}}$  before the rewrite, and the second line is after the rewrite.  $X_{t,g}$  and  $X_{t,l}$  are the output tensors of  $L_t^{\text{global}}$  and  $L_t^{\text{local}}$  respectively.  $X_{r,g}$  and  $X_{r,l}$  are the outputs of  $L_r^{\text{global}}$  and  $L_r^{\text{local}}$ . Tags are omitted because every tensor access refers to the final result of that memory location.

The intuition of why this rewrite gives the correct result is the following: in split-k global section,  $s\_sum\_global$  (which sums over  $\text{sum\_l}$ ) does not read from  $\text{sum\_l}$  too early like in rolling update.  $s\_sum\_global$  executes entirely after the  $s\_sum\_local$  loop nest. The only correctness issue is that the values in  $\text{sum\_l}$  are themselves wrong, because they use incorrect row-max result  $\text{max\_l}$ . Therefore, split-k update only needs to repair every incoming local sum  $\text{sum\_l}$  by tag-updating it to the correct row-max result  $\text{max\_g}$ , which is exactly the rewrite in Eq. 8.

Split-k update provides different tradeoffs from rolling update: split-k offers more parallelism at the cost of a global synchronization in the middle of the program.

## 5 Translating from Loop-scalar IR to Tile IR

The lower part of Figure 4 is an example program in Neptune’s tile IR. This program transposes the input matrix  $\text{inp}$ , applies an element-wise exponential, and computes a row sum. Tile IR consists of tensor tile expressions, tile store statements, and loops. Tile expressions allow broadcasting, element-wise operations, reductions, and dimension permutations. This design aligns with the capabilities of Neptune’s tile optimizers,

```

for i, j in grid(N, M):
    for r, c in grid(R, C):
        exp2d[i*R+r, j*C+c] = exp(inp[j*C+c, i*R+r])
    for r, c in grid(R, C):
        max1d[i*R+r] = max(max1d[i*R+r], exp2d[i*R+r, j*C+c])
    ↓
for i, j in grid(N, M):
    exp2d[i*R : i*R+R, j*C : j*C+C] =
        exp(permute(inp[j*C : j*C+C, i*R : i*R+R]))
    max1d[i*R : i*R+R] = reduce(max, dim=1,
        tile=exp2d[i*R : i*R+R, j*C : j*C+C])

```

**Figure 4.** An example program in Neptune’s tile IR. Neptune translates the program in loop-scalar IR (above) to the program in tile IR (below).

i.e., tile expressions express computation that the tile optimizers can process. We provide the syntax of the tile IR in Appendix E.

Neptune translates a program from the loop-scalar IR to the tile IR, by detecting parts of the program with computation regular enough to express as tile expressions, and converts them into tile store statements. This process is called *tensorization*. Tensorization has been studied extensively in the compiler literature [4, 38, 45], and we here demonstrate how it applies to Neptune’s program with an example. Appendix E discusses how the approach works more formally.

Figure 4 shows the translation process, with the input loop-scalar program above and the output tile program below. In the input program, we focus on the first  $(r,c)$  loop nest that writes to  $\text{exp2d}$ . This inner nest as a whole reads a 2D region and writes a 2D region:  $\text{inp}[j*C:j*C+C, i*R:i*R+R]$  and  $\text{exp2d}[i*R:i*R+R, j*C:j*C+C]$ . For simple element-wise operations, it suffices to substitute these two tiles into the body of the nest. However, for our example, we get that  $\text{exp2d}[i*R:i*R+R, j*C:j*C+C] = \exp(\text{inp}[j*C:j*C+C, i*R:i*R+R])$ , which is incorrect because we forget the transpose operation. We need to *reconcile* the order of loop variables in the loops and in the tile statement. In the loop nest  $(r,c)$ , the  $\text{inp}$  tile is indexed by  $c$  first, then  $r$ , while the  $\text{exp2d}$  tile is indexed by  $r$  then  $c$ . Transposing the  $\text{inp}$  tile to  $(r,c)$  order gives us the correct statement.

The key step of Neptune’s tensorization is dimension order reconciliation. The input to the reconciliation algorithm is an *einops* [32] expression, i.e., Einstein notation extended with general reduction operators. This algorithm is more general than typical tensorization algorithms that do pattern matching to match tile computation with specific hardware features (e.g., detecting transposed input for TensorCore matmuls).

Neptune traverses the loop nests to extract einops expressions from store statements in the input program. In Figure 4, the einops expression is “ $c\ r \rightarrow r\ c$ ” for the first store, and  $\text{reduce}("r\ c \rightarrow r", \text{max})$  for the second. For each operation that involves two tiles, the reconciliation algorithm applies three steps to match their dimension order:

- Broadcasting, to match the lower-dimensional tile to the higher-dimensional tile. In `lhs[r, c]/rhs[r]`, the `rhs` tile misses the `c` dimension, so we broadcast it: `rhs[r, None]`.
- Permutation, to match two orders that have the same dimensions. For our example `einops "c r -> r c"`, we add a `permute(order=(1, 0))` operation to match them.
- Reduction, which only applies to the two sides of an assignment. If the value tile has more dimensions than the assigned tile, we apply the reduce operation to the value tile. For the `einops reduce("r c -> r", max)`, we apply reduction to the `c` (second dimension).

Neptune uses existing tensorization algorithms (built on top of TVM [6]) to find access regions of an inner loop nest, and extracts `einops` expressions to apply reconciliation, which produces the correct tile store statement. It then replaces the entire inner loop nest with this tile store statement, generating a tile program that the underlying tile compiler can optimize.

## 6 Implementation

Neptune is built on top of TVM and Triton tensor compilers. We implement Neptune’s loop-scalar IR and tile IR as extensions of TVM TensorIR. We adapt TVM’s scheduling language as Neptune’s scheduling framework, where we implement Neptune’s transformations such as rolling update. Neptune reuses TVM’s tensor expression language and its translator from tensor expressions to TensorIR. Neptune uses Triton as its tile optimizer and code generator, and Neptune has a translator from its tile IR to Triton’s Python DSL. We use SymPy, a Python library for symbolic equation solving, to implement the algorithm for finding the repair function  $h$  in rolling update and split-k update.

Neptune is implemented in 10K lines of C++ and Python code, with 3K lines for the loop fusion transformations and 1.3K lines for loop-to-tile translation. Neptune adapts TVM MetaSchedule [33] as its autotuner, reusing its search algorithm. We register our transformations with MetaSchedule such that it knows how to work with Neptune schedules. MetaSchedule is a cost model-guided autotuner that repeats the following steps: produce 1024 schedules, predict their performance, and run 16 of them on the target hardware (called **empirical measurements**). Every prediction invokes the template-guided optimizer in Neptune, while every empirical evaluation fully generates the program, applying our loop-to-tile translation and Triton-based tile optimization.

## 7 Experimental Methodology

**Hardware platforms.** We choose four GPU devices for the evaluation: *datacenter devices* Nvidia A100 [10] (SXM4 40 GB version) and AMD MI300; and *desktop devices* Nvidia RTX A5000 and Nvidia RTX 6000 Ada [11, 12].

**Operator Experiments.** We evaluate Neptune on 10 operators shown in Table 1. Each operator is extracted from a specific large language model (LLM) or vision language

**Table 1.** LLM operators used in our evaluation. PF is short for prefill and DC for single-token decoding.

Operator	Description	Base Arch.
Global (PF)	Global (plain) attention	ViT-L/16
Causal (PF/DC)	Attn + causal mask	GPT3 6.7B
ALIBI (PF/DC)	Attn + ALIBI bias + causal mask	MPT 7B
GQA (PF/DC)	Attn + GQA heads + causal mask	LLama3 70B
SoftCap (PF/DC)	Attn + SoftCap bias + GQA heads + causal mask	
Window (PF)	Attn + windowed mask	Gemma2 27B

model (VLM) architecture, shown on the **Base Arch.** column. We profile operators in prefill (PF) mode: where the query sequence length  $s_q$  equals key/value length  $s_{kv}$ , and decoding (DC) mode, where  $s_q = 1$ . Variations on masking (Global, Causal, and Window) are indistinguishable in decoding, so we select the Causal variant out of the three. All operators run in inference mode at float16 (half) precision. We profile these operators at varying sequence lengths:  $2^7 = 128, 2^8 = 256, \dots, 2^{15} = 32768$ , and a batch size of 1 unless otherwise specified. We refer to the triple of operator, input shape, and GPU as a **setup**, and we evaluate  $10 \times 8 \times 4 = 320$  setups. We run Neptune’s autotuner for 128 empirical measurements per setup.

**Baselines.** We list our 10 baselines and underline the names we refer to them with in evaluation. Our baselines include 4 tensor compilers: Triton 3.2, FlexAttention (FlexAttn) 2.6.0, Mirage 0.2.2, and TVM 0.18. Triton requires a user to write the kernel in its frontend language, so we compare three mainstream implementations in Triton: OpenAI Triton [28], Tri-Dao Triton [16], and XFormers Triton [21]. Our baselines also include 4 optimized inference libraries: PyTorch 2.6.0 [30], cuDNN 9.11.0, Tri-Dao Cutlass 2.7.4 (Dao-AI Lab’s implementation) [16], and FlashInfer 0.2.4 [41]. Each implementation supports a subset of the setups we evaluate. For PyTorch, we use `torch.compile(backend='inductor')` to ensure high performance. We evaluate Mirage on A100, on the Global operator over a grid of  $s_q \neq 1$  and  $s_{kv}$ , which is consistent with the evaluation in the Mirage paper.

**Profiling and Performance Reporting.** For any kernel we profile, we run the kernel once to warm up and discard the result, and run 15 times to report the mean latency. We profile the kernels with Nsight Systems (nsys) on Nvidia GPUs and ROCprofiler (rocprofv3) on AMD GPU. Both profilers trace the program and measure the latency of every kernel in the program. We report **speedup** of Neptune over the best baseline: if Neptune’s kernel has mean latency  $t_0$  and the baselines have  $t_1, \dots, t_n$ , then our speedup is  $\min(t_1, \dots, t_n) / t_0$ . We also report **relative performance** of a baseline relative to Neptune, which is  $t_0 / t_i$  for the  $i$ -th baseline. To average these metrics across setups, we compute geometric means (geomeans).

## 8 Evaluation

### 8.1 Neptune vs. Tensor Compilers

**Overall Trends.** Table 2 shows averaged speedup of Neptune over the best compiler baseline, where each cell is a

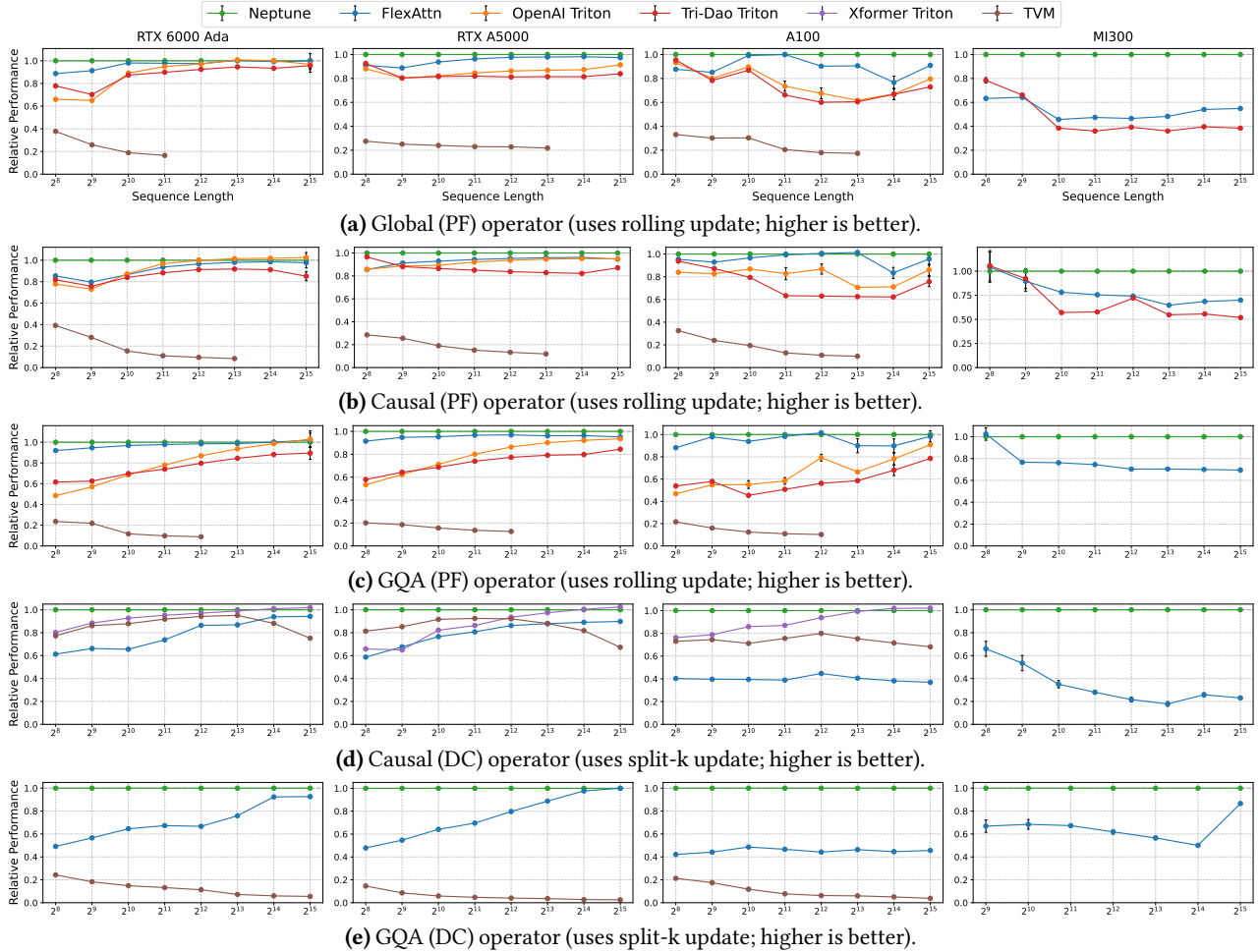


**Figure 5.** Performance of Neptune kernels vs. kernels by other tensor compilers. The y-axis shows relative performance of all compilers normalized to Neptune for each setup. The plots for the remaining benchmarks are in Appendix F.

geomean over input sequence lengths. Out of 320 setups we evaluate, Neptune achieves better or equal performance compared to all other compilers on 284 setups. Neptune shows improvement over the baselines for all four GPU architectures, ranging from  $1.15\times$  to  $1.85\times$ . Neptune shows improvement on all GPUs, indicating the portability of our approach across GPU architectures. Across all setups, Neptune achieves geomean  $1.35\times$  the performance of the best compiler baseline. All kernels for PF benchmarks use Rolling Update, and all kernels for DC benchmarks use Split-K Update.

**Detailed Results for Setups.** Figure 5 presents detailed performance for every setup for five operators that see the most usage in existing LLMs and have the most support in the baselines. Each plot shows relative performance (y-axis) of other compilers normalized to Neptune for different sequence lengths (x-axis).

On Nvidia GPUs, Neptune achieves the best performance in a majority of setups. TVM performance is low for most operators as its fusion legality check forbids reduction fusion,

**Table 2.** Speedup of Neptune relative to the best compiler baseline, for all 10 operators on 4 GPUs.

Operator \ GPU	6000Ada	A5000	A100	MI300
Global (PF)	1.03	1.05	1.10	1.84
Causal (PF)	1.06	1.06	1.05	1.29
GQA (PF)	1.02	1.05	1.06	1.32
Causal (DC)	1.06	1.08	1.11	3.26
GQA (DC)	1.45	1.37	2.21	1.55
ALIBi (PF)	1.56	1.61	1.71	2.02
ALIBi (DC)	1.28	1.27	2.65	3.32
SoftCap (PF)	1.08	1.07	1.03	1.42
SoftCap (DC)	1.08	0.95	1.86	2.55
Window (PF)	1.03	1.02	0.99	1.23
<b>Average</b>	<b>1.15</b>	<b>1.14</b>	<b>1.38</b>	<b>1.85</b>

resulting in multiple kernels with increased memory transfer. Most tile-based implementations show better performance than TVM and improve their performance as sequence length increases. For prefill (PF) operators, Neptune achieves higher

**Table 3.** Speedup of Neptune relative to Mirage on global attention, over a grid of  $s_q$  and  $s_{kv}$  where  $s_q \leq s_{kv}$ . Cells where  $s_q > s_{kv}$  has an em-dash (—). Cells where Mirage fails to find a valid kernel has a cross (X). The GPU is A100.

$s_q$	$s_{kv}$	128	256	512	1024	2048
16	—	1.98	2.25	1.60	1.30	4.10
32	—	2.10	1.44	1.47	1.25	1.39
64	—	1.63	1.92	1.32	1.29	1.58
128	—	X	1.83	2.40	1.63	1.85
256	—	—	2.04	3.35	4.40	6.40
512	—	—	—	3.64	6.01	X
1024	—	—	—	—	6.71	X
2048	—	—	—	—	—	X

performance for shorter sequence lengths. Neptune and FlexAttn benefit from autotuning and have higher performance than other baselines that rely on Triton heuristics.

For the decoding (DC) operators, we evaluate XFormer Triton since two Triton-based kernels (OpenAI, Tri-Dao) do not support it. TVM provides higher performance for Causal (DC) than for other operators, because Causal (DC) is a matrix-vector multiplication operator where fusion has limited effect on its memory-boundness. Neptune delivers consistently better performance on GQA (DC) because it uses masks to apply TensorCore to the dot product in the computation that would otherwise have too few input matrix rows for TensorCore. There is no single baseline that provides high performance like Neptune does across all operators and GPUs.

Only FlexAttn and Tri-Dao Triton (limited to Global and Causal PF) support AMD GPU. While fewer baseline compilers support these operators, Neptune delivers consistent high performance compared to the available baselines.

**Programmability.** Triton-based baselines require a user to write the kernel in their DSL, and FlexAttn uses multiple attention-specific templates developed by the framework authors. For instance, the Tri-Dao Triton kernel is 650 lines of code, while Neptune’s input is vanilla attention (38 lines) and schedule (28 lines) in total; see Appendix A for these inputs.

**Mirage Superoptimizer.** We discuss Mirage separately, as we have observed that Mirage does not consistently find valid kernels for all input shapes and only supports variants of Global and Causal operators. Table 3 shows the speedup of Neptune relative to Mirage. The columns and rows vary by  $s_{kv}$  and  $s_q$  respectively, where  $s_q \leq s_{kv}$ . Cells where  $s_q > s_{kv}$  are filled with an em dash (—), while cells where Mirage fails to find a valid kernel have a cross (X). The results show 2.21x lower latency (geomean) across all tested shapes, while Neptune provides deterministic correctness guarantees (unlike Mirage’s probabilistic), and we observed better numerical accuracy with Neptune.

## 8.2 Neptune vs. Manually Optimized Libraries

Table 4 shows the performance of Neptune kernels vs. kernels from manually optimized libraries. The y-axis shows average

**Table 4.** Speedup of Neptune relative to the best manually optimized library baseline, for 10 operators on 4 GPUs. Each cell is an average over input sequence lengths.

GPU Operator	6000Ada	A5000	A100	MI300
Global (PF)	0.96	0.95	0.84	0.93
Causal (PF)	0.97	0.89	0.81	0.68
GQA (PF)	0.93	0.85	0.80	0.64
Causal (DC)	0.99	0.98	0.99	5.32
GQA (DC)	1.09	1.17	1.24	2.14
ALiBi (PF)	1.65	1.36	1.24	0.98
ALiBi (DC)	1.07	1.12	1.17	5.71
Window (PF)	0.85	0.67	0.70	0.46
<b>Average</b>	1.04	0.98	0.95	1.36

relative performance: each framework’s performance relative to Neptune, averaged over sequence lengths. The error bar depicts the range of relative performance over sequence lengths: if a framework does better on some shapes and worse on others, it will have a large error bar. Figure 4 omits the SoftCap operator (both prefill and decoding), because existing baseline libraries do not support it. Therefore, this figure shows  $4 \times 8 \times 8 = 256$  setups.

Out of 256 setups, Neptune has better or equal performance compared to all libraries on 101 setups. On average of all setups, Neptune delivers geommean 1.07x the performance of the best library baseline. There is not a single library that consistently delivers the best performance or outperforms Neptune on all setups. For example, cuDNN has the highest performance on most short-sequence setups, and low performance for long sequences. In contrast, CUTLASS implementations have higher performance on longer sequences for many operators, such as Global (PF) and GQA (DC). Appendix F Figure 16 shows these trends over all input shapes.

The high performance of kernel libraries is a result of manual optimization: they show better performance on operators that are more commonly used (Global, Causal and GQA PF) and on more popular GPUs (e.g. A100), and lower performance than Neptune otherwise. Neptune failed to optimize Window (PF) because its TVM-based loop analysis could not identify the proper condition for loop partitioning.

## 8.3 Scalability Test

Optimizations in Neptune involve various trade-offs that introduce a small amount of resource overhead, such as register and shared memory (SMEM) usage, for significant performance gains. To show that Neptune’s resource usage is acceptable, we stress test Neptune on increasing batch sizes until we reach the limit of available GPU memory. Figure 6 shows the throughput (in TFLOPs/sec) of Neptune’s kernel and multiple baselines for the GQA (PF) operator on RTX A5000. We use a sequence length of 8192 as it allows us to test more batch sizes up to 32. The throughput of all kernels decreases as input size increases, as longer workloads are more likely to trigger GPUs’ clock and power throttling.

Neptune’s kernel remains close to the best implementation (slightly behind cuDNN) for all the batch sizes we test.

We also directly measure the number of registers, SMEM, and global memory used in Neptune’s kernels. On average over all the Nvidia GPU setups, Neptune uses  $0.68\times$  the registers of the baseline that uses the most registers, and  $47\%$  the SMEM of the baseline that uses the most SMEM. The number of registers and amount of SMEM mainly depend on the operator and change little over input size. We did not observe that they have negative impact on speed.

#### 8.4 Ablation Studies

To understand the impact of each component of Neptune, we perform ablation studies on the performance of Neptune’s kernels. We select the Global and Causal operators in prefill with sequence length 512 on RTX 6000 Ada. Figure 7 shows the results of this experiment. On the left, we start from baseline TVM with no Neptune components. As we move to the right, we first add Neptune’s tile optimizations, then Neptune’s fusion algorithms, and finally Neptune’s autotuner. For both operators, fusion is the most impactful optimization, and autotuning provides major improvement for Global and little for Causal. Overall, the effect of the first three steps is consistent over operators and sequence lengths.

## 9 Related Work

**Manual Tensor Operators.** FlashAttention [14] details an attention algorithm with insights similar to a specialized form of rolling update, fusing softmax with matmul through a repair computation. FlashDecoding [15] outlines an attention-specific algorithm that splits the computation into two reduction kernels, similar to applying split-k update. These works present the final operators rather than a general means of transforming operators: a library [16] offers kernels for common attention variants, but specialized variants require their own manual implementations. FlexAttention [17] extends FlashAttention to be parametric on a mask and an element-wise function over the score matrix (the QK product). FlexAttention has better coverage for attention variants but does

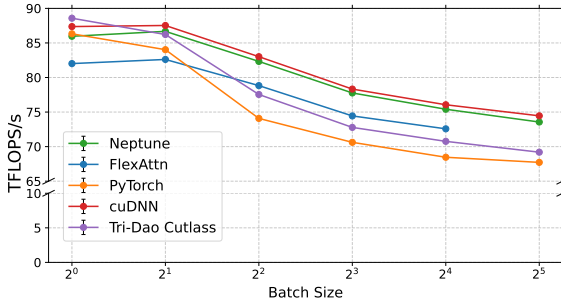


**Figure 6.** Throughput of Neptune kernels and multiple baselines over increasing batch sizes, evaluated on RTX A5000 for the GQA (PF) operator. The y-axis shows throughput in TFLOPS/sec, and the x-axis shows batch size.

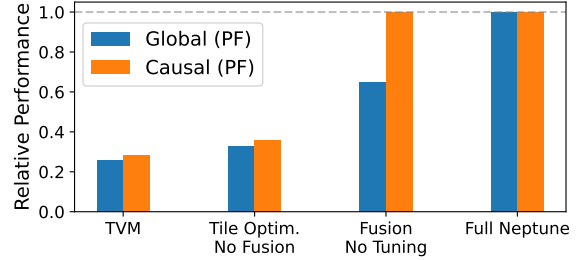


**Figure 7.** Ablation studies of the Neptune kernel performance on sequence length 512 on RTX 6000 Ada. The x-axis labels mark the component of Neptune we keep and remove.

not extend to non-attention operators, and it uses multiple manually optimized templates to generate kernels.

**Tile-Based Compilers.** Many tensor compilers and programming frameworks decompose tensor-level operations into operations over tensor tiles, which often map directly to the underlying hardware. Triton [36], for example, expresses computation in terms of tiles mapping to GPU processor blocks, and Roller [47] recursively tiles kernels to match unknown accelerator architectures. Programming frameworks like [3, 27, 35] provide tiles as a core abstraction and map them to target devices like GPU TensorCores. Tile frameworks automate much of low-level intra-tile optimization, but leave the burden of high-level inter-tile optimization like work distribution, scheduling, and operator fusion to the programmer.

**Scheduling Kernel Compilers.** Scheduling compilers like Halide [31], TVM [6], and others [18, 46] separate the specification and implementation of a tensor operator, allowing transformations like loop tiling and fusion to be specified in an external schedule. Scheduling allows the programmer to compose optimizations using their domain expertise, but the number of steps required to reach a high-performance kernel can overwhelm programmers. Many scheduling compilers, such as extensions of TVM and Halide, provide some automation for schedule creation, but they fall short on computation-editing transformations like Neptune provides.

**Graph- and Model-level Compilers.** Beyond single operators, many frameworks like PyTorch [30], XLA/HLO [29], TVM [6], and others [1, 26, 31, 39] describe tensor programs as operator graphs, and apply graph-level optimizations. These graph-level frameworks implement operator fusion through epilogue-visitor trees [7] or manually defined fusion rules based on access patterns [26]. These operator fusion methods lack the flexibility that scheduling provides. Moreover, they ensure correctness by preserving dependencies, which as we have demonstrated, is insufficient to realize reduction fusion like rolling update that requires algebraic manipulation. Many frameworks [19, 20, 25, 31, 37, 40] including XLA [29], TVM [6], and TASO [19] perform rewrites on tensor graphs. Graph-level frameworks commonly work at the operator level though, and struggle to express the loop or tile level transformations necessary for rolling update.

**Superoptimization Compilers.** Some tensor compilers apply superoptimization, which transforms the given tensor program in ways that may not preserve equivalence, and impose additional checks to select implementations that produce the correct result. *Mirage* [39] is a hierarchical superoptimizer that jointly transforms the program at thread, tile, and operator levels. For correctness, *Mirage* uses a statistical equivalence procedure, based on sampling and acceptance probability threshold. It runs the candidate program over inputs sampled from two integer finite fields and checks if the outputs are equal. In contrast, *Neptune*’s correctness guarantee is fully deterministic, in the style of traditional compiler optimizations. The search algorithm in *Mirage* can take minutes to hours, and it may fail to find valid kernels or find kernels with unpredictable performance, all of which we have observed in experiments in Section 8.

**ML Autotuners.** Many machine learning frameworks adopt autotuning to improve the performance of ML workloads. Tensor compilers use autotuners to search for high-performance tensor programs on specific hardware, such as [2, 22, 24] in Halide, and Ansor [44] and MetaSchedule [33] in TVM. Felix [42] is a tensor compiler that uses gradient descent to search for high-performance tensor programs, which differs from the traditional discrete autotuning used in other tensor compilers. Triton [36] tensor programming language provides an autotuning search method while leaving the tuning knob definitions to the user. Autotuning is also used to explore trade-offs between performance and accuracy of deep learning models, in frameworks that apply accuracy-aware optimizations [34, 43].

## 10 Conclusion

We presented *Neptune*, a novel tensor compiler for advanced operator fusion. *Neptune* shows, for the first time, that fusion algorithms that can be included in a standard compiler schedule can find kernels with performance equal or higher than that of Triton versions of manually optimized attention kernels like FlashAttention and FlashDecoding, and comparable to their CUTLASS versions.

*Neptune* opens a new direction toward bringing such optimizations fully within the scope of optimizing tensor compilers. We anticipate that this integration can pave the way for automatic discovery of new efficient advanced ML operators.

## Acknowledgments

This research was supported in part by the National Science Foundation Grant No. CCF-2217144 and the IBM-Illinois Discovery Accelerator Institute.

## References

- [1] Martín Abadi, Paul Barham, Jianmin Chen, Zhifeng Chen, Andy Davis, Jeffrey Dean, Matthieu Devin, Sanjay Ghemawat, Geoffrey Irving, Michael Isard, et al. {TensorFlow}: a system for {Large-Scale} machine learning. In *12th USENIX symposium on operating systems design and implementation (OSDI 16)*, pages 265–283, 2016.
- [2] Andrew Adams, Karima Ma, Luke Anderson, Riyadh Baghdadi, Tzu-Mao Li, Michaël Gharbi, Benoit Steiner, Steven Johnson, Kayvon Fatahalian, Frédéric Durand, and Jonathan Ragan-Kelley. Learning to optimize halide with tree search and random programs. *ACM Transactions on Graphics (TOG)*, 38, 2019.
- [3] The JAX Authors. Pallas: a jax kernel language. <https://docs.jax.dev/en/latest/pallas/index.html>, 2024.
- [4] Somashekharacharya G. Bhaskaracharya, Julien Demouth, and Vinod Grover. Automatic kernel generation for volta tensor cores. *CoRR*, abs/2006.12645, 2020.
- [5] W. Blume and R. Eigenmann. Nonlinear and symbolic data dependence testing. *IEEE Transactions on Parallel and Distributed Systems*, 9(12):1180–1194, 1998.
- [6] Tianqi Chen, Thierry Moreau, Ziheng Jiang, Haichen Shen, Eddie Q. Yan, Leyuan Wang, Yuwei Hu, Luis Ceze, Carlos Guestrin, and Arvind Krishnamurthy. TVM: end-to-end optimization stack for deep learning. *CoRR*, abs/1802.04799, 2018.
- [7] Zhaodong Chen, Andrew Kerr, Richard Cai, Jack Kosaian, Haicheng Wu, Yufei Ding, and Yuan Xie. Evt: Accelerating deep learning training with epilogue visitor tree. In *Proceedings of the 29th ACM International Conference on Architectural Support for Programming Languages and Operating Systems, Volume 3, ASPLOS ’24*, page 301–316, 2024.
- [8] Chillee. Where do the 2000+ pytorch operators come from? (pytorch developer discussions). <https://dev-discuss.pytorch.org/t/where-do-the-2000-pytorch-operators-come-from-more-than-you-wanted-to-know/373>.
- [9] NVIDIA Corporation. NVIDIA cuSPARSElt. <https://docs.nvidia.com/cuda/cusparselt/types.html>, 2021.
- [10] NVIDIA Corporation. NVIDIA A10 Tensor Core GPU. <https://www.nvidia.com/en-us/data-center/a100/>, 2024.
- [11] NVIDIA Corporation. NVIDIA RTX 6000 Ada-generation Graphics Card. <https://www.nvidia.com/en-us/design-visualization/rtx-6000/>, 2024.
- [12] NVIDIA Corporation. NVIDIA RTX A5000 Graphics Card. <https://www.nvidia.com/en-us/design-visualization/rtx-a5000/>, 2024.
- [13] Tri Dao. FlashAttention-2: Faster attention with better parallelism and work partitioning. In *International Conference on Learning Representations (ICLR)*, 2024.
- [14] Tri Dao, Dan Fu, Stefano Ermon, Atri Rudra, and Christopher Ré. Flashattention: Fast and memory-efficient exact attention with io-awareness. *Advances in neural information processing systems*, 35:16344–16359, 2022.
- [15] Tri Dao, Grigory Sizov, Francisco Massa, and Daniel Haziza. Flash-decoding for long-context inference, Oct 2023.
- [16] Dao-AILab. FlashAttention. <https://github.com/Dao-AILab/flash-attention>, 2023.
- [17] Juechu Dong, Boyuan Feng, Driss Guessous, Yanbo Liang, and Horace He. Flex attention: A programming model for generating optimized attention kernels, 2024.
- [18] Siyuan Feng, Bohan Hou, Hongyi Jin, Wuwei Lin, Junru Shao, Ruihang Lai, Zihao Ye, Lianmin Zheng, Cody Hao Yu, Yong Yu, et al. Tensorir: An abstraction for automatic tensorized program optimization. In *Proceedings of the 28th ACM International Conference on Architectural Support for Programming Languages and Operating Systems, Volume 2*, pages 804–817, 2023.
- [19] Zhihao Jia, Oded Paden, James Thomas, Todd Warszawski, Matei Zaharia, and Alex Aiken. Taso: optimizing deep learning computation with automatic generation of graph substitutions. In *Proceedings of the 27th ACM Symposium on Operating Systems Principles*, pages 47–62, 2019.
- [20] Zhihao Jia, James Thomas, Todd Warszawski, Mingyu Gao, Matei Zaharia, and Alex Aiken. Optimizing dnn computation with relaxed graph substitutions. *Proceedings of Machine Learning and Systems*,

- [21] Benjamin Lefadeux, Francisco Massa, Diana Liskovich, Wenhan Xiong, Vittorio Caggiano, Sean Naren, Min Xu, Jieru Hu, Marta Tintore, Susan Zhang, Patrick Labatut, Daniel Haziza, Luca Wehrstedt, Jeremy Reizenstein, and Grigory Sizov. xformers: A modular and hackable transformer modelling library. <https://github.com/facebookresearch/xformers>, 2022.
- [22] Tzu-Mao Li, Michaël Gharbi, Andrew Adams, Frédéric Durand, and Jonathan Ragan-Kelley. Differentiable programming for image processing and deep learning in halide. *ACM Trans. Graph.*, 37(4), 2018.
- [23] Aaron Meurer, Christopher P. Smith, Mateusz Paprocki, Ondřej Čertík, Sergey B. Kirpichev, Matthew Rocklin, AMiT Kumar, Sergiu Ivanov, Jason K. Moore, Sartaj Singh, Thilina Rathnayake, Sean Vig, Brian E. Granger, Richard P. Muller, Francesco Bonazzi, Harsh Gupta, Shivam Vats, Fredrik Johansson, Fabian Pedregosa, Matthew J. Curry, Andy R. Terrel, Štěpán Roučka, Ashutosh Saboo, Isuru Fernando, Sumith Kulal, Robert Cimrman, and Anthony Scopatz. Sympy: symbolic computing in python. *PeerJ Computer Science*, 3:e103, January 2017.
- [24] Ravi Teja Mullapudi, Andrew Adams, Dillon Sharlet, Jonathan Ragan-Kelley, and Kayvon Fatahalian. Automatically scheduling halide image processing pipelines. *ACM Trans. Graph.*, 35(4), jul 2016.
- [25] Julie L. Newcomb, Andrew Adams, Steven Johnson, Rastislav Bodik, and Shoib Kamil. Verifying and improving halide’s term rewriting system with program synthesis. *Proc. ACM Program. Lang.*, 4(OOPSLA), November 2020.
- [26] Wei Niu, Jie Xiong, Guan, Yanzhi Wang, Gagan Agrawal, and Bin Ren. Dnnfusion: accelerating deep neural networks execution with advanced operator fusion. In *Proceedings of the 42nd ACM SIGPLAN International Conference on Programming Language Design and Implementation*, PLDI 2021, page 883–898, 2021.
- [27] NVIDIA. CUTLASS: CUDA Templates for Linear Algebra Subroutines. <https://github.com/NVIDIA/cutlass>, 2021.
- [28] OpenAI. Fused Attention – Triton Documentation. <https://triton-lang.org/main/getting-started/tutorials/06-fused-attention.html>, 2024.
- [29] OpenXLA. Xla. <https://openxla.org/xla>.
- [30] Adam Paszke, Sam Gross, Francisco Massa, Adam Lerer, James Bradbury, Gregory Chanan, Trevor Killeen, Zeming Lin, Natalia Gimelshein, Luca Antiga, et al. Pytorch: An imperative style, high-performance deep learning library. *Advances in neural information processing systems*, 32, 2019.
- [31] Jonathan Ragan-Kelley, Connnelly Barnes, Andrew Adams, Sylvain Paris, Frédéric Durand, and Saman Amarasinghe. Halide: A language and compiler for optimizing parallelism, locality, and recomputation in image processing pipelines. In *ACM SIGPLAN Conference on Programming Language Design and Implementation*, 2013.
- [32] Alex Rogozhnikov. Einops: Clear and versatile tensor manipulations for deep learning. <https://github.com/argozhnikov/einops>, 2020. GitHub repository, Accessed: [Date Accessed].
- [33] Junru Shao, Xiyou Zhou, Siyuan Feng, Bohan Hou, Ruihang Lai, Hongyi Jin, Wuwei Lin, Masahiro Masuda, Cody Hao Yu, and Tianqi Chen. Tensor program optimization with probabilistic programs. In *Advances in Neural Information Processing Systems*, volume 35, 2022.
- [34] Hashim Sharif, Yifan Zhao, Maria Kotsifakou, Akash Kothari, Ben Schreiber, Elizabeth Wang, Yasmin Sarita, Nathan Zhao, Keyur Joshi, Vikram S Adve, Sasa Misailovic, and Sarita V Adve. Approxcaliper: a compiler and runtime system for adaptive approximations. In *Proceedings of the 26th ACM SIGPLAN Symposium on Principles and Practice of Parallel Programming*, 2021.
- [35] Benjamin F. Spector, Simran Arora, Aaryan Singhal, Daniel Y. Fu, and Christopher Ré. Thunderkittens: Simple, fast, and adorable ai kernels, 2024.
- [36] Philippe Tillet, H. T. Kung, and David Cox. Triton: an intermediate language and compiler for tiled neural network computations. In *Proceedings of the 3rd ACM SIGPLAN International Workshop on Machine Learning and Programming Languages*, page 10–19, June 2019.
- [37] Haojie Wang, Jidong Zhai, Mingyu Gao, Zixuan Ma, Shizhi Tang, Liyan Zheng, Yuanzhi Li, Kaiyuan Rong, Yuanyong Chen, and Zhihao Jia. PET: Optimizing tensor programs with partially equivalent transformations and automated corrections. In *15th USENIX Symposium on Operating Systems Design and Implementation (OSDI 21)*, pages 37–54, July 2021.
- [38] Jian Weng, Animesh Jain, Jie Wang, Leyuan Wang, Yida Wang, and Tony Nowatzki. Unit: Unifying tensorized instruction compilation. In *2021 IEEE/ACM International Symposium on Code Generation and Optimization (CGO)*, page 77–89, February 2021.
- [39] Mengdi Wu, Xinhao Cheng, Shengyu Liu, Chunran Shi, Jianan Ji, Man Kit Ao, Praveen Velliyigiri, Xupeng Miao, Oded Padon, and Zhihao Jia. Mirage: A {Multi-Level} superoptimizer for tensor programs. In *19th USENIX Symposium on Operating Systems Design and Implementation (OSDI 25)*, pages 21–38, 2025.
- [40] Yichen Yang, Phitchaya Phothilimthana, Yisu Wang, Max Willsey, Sudip Roy, and Jacques Pienaar. Equality saturation for tensor graph superoptimization. In A. Smola, A. Dimakis, and I. Stoica, editors, *Proceedings of Machine Learning and Systems*, volume 3, pages 255–268, 2021.
- [41] Zihao Ye, Lequn Chen, Ruihang Lai, Wuwei Lin, Yineng Zhang, Stephanie Wang, Tianqi Chen, Baris Kasikci, Vinod Grover, Arvind Krishnamurthy, and Luis Ceze. Flashinference: Efficient and customizable attention engine for llm inference serving. *arXiv preprint arXiv:2501.01005*, 2025.
- [42] Yifan Zhao, Hashim Sharif, Vikram Adve, and Sasa Misailovic. Felix: Optimizing tensor programs with gradient descent. In *Proceedings of the 29th ACM International Conference on Architectural Support for Programming Languages and Operating Systems, Volume 3*, ASPLOS ’24, page 367–381, 2024.
- [43] Yifan Zhao, Hashim Sharif, Peter Pao-Huang, Vatsin Ninad Shah, Arun Narenthiran Sivakumar, Mateus Valverde Gasparino, Abdulrahman Mahmoud, Nathan Zhao, Sarita Adve, Girish Chowdhary, Sasa Misailovic, and Vikram Adve. Approxcaliper: A programmable framework for application-aware neural network optimization. In *Proceedings of Machine Learning and Systems 5*, 2023.
- [44] Lianmin Zheng, Chengfan Jia, Minmin Sun, Zhao Wu, Cody Hao Yu, Ameer Haj-Ali, Yida Wang, Jun Yang, Danyang Zhuo, Koushik Sen, Joseph E. Gonzalez, and Ion Stoica. Ansor: Generating high-performance tensor programs for deep learning. In *USENIX Conference on Operating Systems Design and Implementation*, OSDI’20, 2020.
- [45] Size Zheng, Renze Chen, Anjiang Wei, Yicheng Jin, Qin Han, Liqiang Lu, Bingyang Wu, Xiuhong Li, Shengen Yan, and Yun Liang. Amos: enabling automatic mapping for tensor computations on spatial accelerators with hardware abstraction. In *Proceedings of the 49th Annual International Symposium on Computer Architecture*, ISCA ’22, page 874–887, 2022.
- [46] Size Zheng, Yun Liang, Shuo Wang, Renze Chen, and Kaiwen Sheng. Flextensor: An automatic schedule exploration and optimization framework for tensor computation on heterogeneous system. In *Proceedings of the Twenty-Fifth International Conference on Architectural Support for Programming Languages and Operating Systems*, ASPLOS ’20, page 859–873, 2020.
- [47] Hongyu Zhu, Ruofan Wu, Yijia Diao, Shanbin Ke, Haoyu Li, Chen Zhang, Jilong Xue, Lingxiao Ma, Yuqing Xia, Wei Cui, Fan Yang, Mao Yang, Lidong Zhou, Asaf Cidon, and Gennady Pekhimenko. ROLLER: Fast and efficient tensor compilation for deep learning. In *16th USENIX Symposium on Operating Systems Design and Implementation (OSDI 22)*, pages 233–248, July 2022.

## A Neptune Inputs

Neptune takes as input a compute definition of the operator to optimize, and a schedule that describes how to optimize the operator.

Figure 8 shows a flexible compute definition for attention that Neptune takes as input. It allows customizing bias and mask conditions, and in 38 lines of code it covers all operators in Table 1 except GQA operators.

Figure 9 shows the schedule that pairs with the compute definition. In 28 lines of code, it applies rolling update to fuse the attention computation into a single loop nest, and produces many of the high-performance kernels in our evaluation.

```

1  def create_general_attention(
2      B: int, N: int, QS: int, KVS: int, H: int,
3      mask_cond: Callable,
4      score_mod: Callable,
5  ):
6      q = placeholder((B, N, QS, H), "float16", name="q")
7      k = placeholder((B, N, KVS, H), "float16", name="k")
8      v = placeholder((B, N, KVS, H), "float16", name="v")
9      p = batch_matmul(q, k, trans_b=True, out_dtype="float32")
10     score = compute(
11         p.shape, lambda *ax: if_then_else(
12             mask_cond(*ax), score_mod(p(*ax), *ax), float("-inf")),
13             name="score_mod",
14         )
15     j = reduce_axis((0, KVS), name="j")
16     s_max = compute(
17         (B, N, QS), lambda b, n, i: max(score(b, n, i, j), axis=j),
18         name="softmax_maxelem"
19     )
20     s_exp = compute(
21         (B, N, QS, KVS),
22         lambda b, n, i, j: exp(score(b, n, i, j) - s_max(b, n, i)),
23         name="softmax_exp",
24     )
25     s_expsum = compute(
26         (B, N, QS), lambda b, n, i: sum(s_exp(b, n, i, j), axis=j),
27         name="softmax_expsum"
28     )
29     s_exp = compute(
30         p.shape, lambda *axes: s_exp(*axes).astype(q.dtype),
31         name="softmax_exp_f16"
32     )
33     sv = batch_matmul(s_exp, v, trans_b=False, out_dtype="float32")
34     sv = compute(
35         sv.shape, lambda b, n, i, j: sv(b, n, i, j) / s_expsum(b, n, i),
36         name="softmax_norm"
37     )
38     return compute(sv.shape, lambda *i: sv(*i).astype(q.dtype), "cast")

```

**Figure 8.** Compute definition for the attention operator, which Neptune takes as input. This definition covers all operators in Table 1 except GQA operators.

```

1  def schedule_attn_with_rolling_update(sch: Schedule):
2      b0 = sch.get_block("batch_matmul_1")
3      b1 = sch.get_block("T_score_mod")
4      b2 = sch.get_block("T_softmax_maxelem")
5      b3 = sch.get_block("T_softmax_exp")
6      b4 = sch.get_block("T_softmax_exp_cast")
7      b5 = sch.get_block("T_batch_matmul_NN")
8      b6 = sch.get_block("T_softmax_expsum")
9      b7 = sch.get_block("T_softmax_norm")
10     b8 = sch.get_block("T_cast")
11     *axes, i, j, k = sch.get_loops(b0)
12     i0, j0 = sch.tile([i, j], [128, 32])
13     sch.compute_at(sch.cache_read(b0, 0, "shared"), i0)
14     sch.bind_block_idx(
15         [*axes, i0],
16         ["blockIdx.x", "blockIdx.y", "blockIdx.z"]
17     )
18     sch.reverse_compute_at(b1, j0)
19     b2rf = sch.rolling_update(b2, j0, factor_axis=0)
20     b6rf = sch.rolling_update(b6, j0, factor_axis=0)
21     b5rf = sch.rolling_update(b5, j0, factor_axis=0)
22     sch.reverse_compute_at(b7, i0)
23     sch.reverse_compute_at(b8, i0)
24     for blk in [b0, b1, b2, b2rf, b3, b4, b5, b5rf, b6, b6rf, b7]:
25         sch.set_scope(blk, 0, "shared")
26     sch.split_scan_buffer(b2, j0, 0)
27     sch.decompose_reduction(b5, j0)
28     sch.decompose_reduction(b6, j0)

```

**Figure 9.** Schedule for the attention operator, which Neptune takes as input. This schedule pairs with the compute definition in Figure 8.

## B Background

**Loop Nest Notation in Neptune IR.** Program snippets in Figures 1a-1c show examples of loops in Neptune’s loop-scalar IR. A loop in this IR is defined by an iteration variable, an upper bound, and a body. Neptune normalizes the range of loops to start from 0 without loss of generality.

In equations, we use a compact notation for loop nests in this IR:  $\text{nest}(\mathbf{i} : \mathbf{n})\{s\}$  to represent  $K$  perfectly nested loops with iteration variables  $\mathbf{i} := (i_1, \dots, i_K)$  and upper bounds  $\mathbf{n} := (n_1, \dots, n_K)$ , and loop body  $s$ . For example,  $\text{nest}((i_1, i_2) : (n_1, n_2))\{s_1, s_2\}$  is equivalent to

```
1 for i1 in range(n1):
2   for i2 in range(n2):
3     s1; s2
```

$\mathbf{i} \in \mathbb{Z}^K$  is the iteration vector of the loop nest. Iteration vectors from the same loop nest are comparable via the lexicographic order:  $\mathbf{i}_1 \prec \mathbf{i}_2$  if  $\mathbf{i}_1$  is lexicographically less than  $\mathbf{i}_2$ .  $\mathbf{n}$  is the upper bound of the loop nest. The iteration domain of the loop nest is an axis-aligned box between 0 and  $\mathbf{n}$ :  $\mathcal{D}^s = \{\mathbf{i} \in \mathbb{Z}^K \mid 0 \leq \mathbf{i} \leq \mathbf{n}\} =: \text{box}(0, \mathbf{n})$ . We adopt the closed interval convention when discussing iteration vectors. We denote the previous iteration of  $\mathbf{i}$  as  $\text{prev}(\mathbf{i})$ , which is the maximum of all iteration vectors smaller than  $\mathbf{i}$ :  $\text{prev}(\mathbf{i}) := \text{lexmax}(\{\mathbf{i}' \in \mathcal{D}^s \mid \mathbf{i}' \prec \mathbf{i}\})$ . Similarly,  $\text{next}(\mathbf{i})$  is the next iteration of  $\mathbf{i}$ .

We may also omit the upper bounds and the body of the loop nest if unused in the context, so  $\text{nest}(\mathbf{i})$ ,  $\text{nest}(\mathbf{i})\{s\}$  and  $\text{nest}(\mathbf{i} : \mathbf{n})$  are valid notations for a loop nest. We refer to a loop in a given loop nest by its iteration variable:  $i_k$  in  $\text{nest}(\mathbf{i} : \mathbf{n})\{s\}$  is the  $k$ -th loop in the nest.

**Affine Access Function and Tags.** Array loads and stores in Neptune IR use affine access functions [5] to index array elements. In an array access  $X[\phi(\mathbf{i})]$ ,  $X$  is the array being accessed, and  $\phi$  is the affine access function that projects the iteration vector  $\mathbf{i}$  to array indices. Since  $\phi$  is affine, we can fully describe it with a matrix  $A$  and a vector  $b$ :

$$\phi: \mathbb{Z}^N \rightarrow \mathbb{Z}^M \quad \phi(\mathbf{i}) = A\mathbf{i} + b$$

$\phi$  is not injective in general. For example, in Figure 1b, the array store  $\text{xsum}[\mathbf{i}]$  has an access function of  $\phi(i, j) = i$ . It is then difficult to refer to the value of  $\text{xsum}[\mathbf{i}]$  at different  $j$ -iterations. In such cases, we add a *tag* to the array access to mark which  $j$ -iteration the access is referring to:  $X[\phi(\mathbf{i})]^{(j)}$  ( $\text{xsum}[\mathbf{i}]^{(j)}$  for the example above). Tags reflect temporal data dependency on the same memory location. They convey the same idea as Figure 1e duplicating the arrays  $\text{xsum}$  and  $\text{xmax}$  to show their value over time.

**Reduce Loop Nest.** A reduce loop nest is a loop nest that expresses a reduction operation. In Neptune IR, a reduce loop nest consists of map loops and reduce loops, where the output is only indexed by the map loop variables, and each output value is updated as many times as the reduce loops execute. For example, the  $\text{s\_sum}$  loop nest in Figure 1a is a reduce loop nest, with one map loop  $i$  and one reduce loop  $j$ . The output

array  $\text{xsum}$  is only indexed by  $i$ , and each value of  $\text{xsum}[i]$  is updated 4 times.

To distinguish reduce loops and map loops, we use the specialized loop nest notation  $\text{rnest}(\mathbf{i} : \mathbf{n}, j : \mathbf{m})\{s\}$  for a reduce loop nest. Therefore, a reduce loop nest has the form

$$\text{rnest}(\mathbf{i} : \mathbf{n}, j : \mathbf{m})\{ X[\phi(\mathbf{i})] = X[\phi(\mathbf{i})] \mathcal{f} \text{expr}(\mathbf{i}, j) \} \quad (9)$$

$f$  is the reducer (an associative binary function),  $a \mathcal{f} b$  is the infix form of  $f(a, b)$ , and  $\text{expr}(\mathbf{i}, j)$  is the values being reduced over that depend on  $i$  and  $j$ .

**Recurrent and Explicit Forms.** Reduce loop nests in Neptune that match Equation 9 updates the output array  $X$  iteratively. We refer to Equation 9 as the *recurrent form* for the value of  $X$ , and it is useful to have a closed-form expression for it. We define the reduce operator  $\mathcal{R}$  that accepts 3 arguments: a reducer  $f$ , a range to reduce over, and the expression to reduce over. For instance,  $\mathcal{R}(+, 0 \leq j \leq 2, \text{xexp}[i, j])$  equals  $\text{xexp}[i, 0] + \text{xexp}[i, 1] + \text{xexp}[i, 2]$ . We refer to this reduce operator-based expression as the *explicit form* for the value of  $X$ .

**Dataflow Analysis.** Neptune performs dataflow analysis at the loop nest level. A loop nest  $L$  is a *producer* of another loop nest  $L_0$  if  $L$  writes to arrays that  $L_0$  reads from, and  $L_0$  is a *consumer* of  $L$ . Producer-consumer relation between loop nests forms a graph, which we call the dataflow graph. A loop nest  $L$  is a predecessor of  $L_0$  if  $L$  is reachable from  $L_0$  on the dataflow graph.

**Naive Loop Fusion.** Loop fusion is a standard transformation in compiler literature that fuses multiple loop nests into a single nest. Neptune uses the Halide-style [31] loop fusion algorithm (known as compute-at in Halide). We modify its data dependency checks such that it no longer validates temporal (tag) data dependency. Data dependency checks based on memory location is still in effect. This modified algorithm is the *naive loop fusion* algorithm used in Neptune.

Naive loop fusion takes a loop nest  $L_0 := \text{nest}(\mathbf{i})\{s\}$  to fuse and a loop  $l$  to fuse  $L_0$  under:  $\text{NaiveLoopFusion}(L_0, l)$ .  $l$  and any loops outside of it are together denoted as a loop nest  $L$ . Naive loop fusion moves  $L_0$  under  $L$ , and cuts the loop ranges of  $L_0$  based on the ranges of  $L$  and memory location dependency. The modified loop nest  $L'_0$  sits under  $L$  and still contains the statement  $s$ . We refer to  $L$  as the outer loop nest and  $L'_0$  as the remainder loop nest of the fusion.

**Array Tile.** A tile of an array is a multi-dimensional subarray. For an array  $X$  of  $K$  dimensions and shape  $m_1, \dots, m_K$ , a tile of  $X$  is an axis-aligned box  $[l_1, u_1] \times \dots \times [l_K, u_K]$  where  $l_k, u_k \in \mathbb{Z}$  and  $0 \leq l_k < u_k < m_k$  for all  $k$ . A tile of  $X$  may have fewer or more dimensions than  $X$ . Neptune’s tile IR has a syntax for removing and inserting dimensions of size 1 on the tile.

## C Step-By-Step Algorithm Application on Motivational Example

Here we include the detailed steps of our rolling update algorithm for the example from Figure 1a.

### C.1 Rolling Update

```

1  # s_max:
2  for i in range(2):           1  for i in range(2):
3      for j in range(4): # loop_j 2      for j in range(4): # loop_j
4          xmax[i] = max(      3          # s_max:
5              xmax[i], inp[i, j]) 4          xmax[i] = max(
6  # s_sum:                   5              xmax[i], inp[i, j])
7  for i, j in grid(2, 4)      6      # s_sum:
8      xsum[i] = xsum[i] + exp( 7          xsum[i] = xsum[i] + exp(
9          inp[i, j] - xmax[i]) 8              inp[i, j] - xmax[i])

```

- (a) Step 1: dataflow reorganization. This step inlines  $s_{\text{exp}}$  (into  $s_{\text{sum}}$ ) and loop fusion fuses  $s_{\text{sum}}$  and  $s_{\text{max}}$  under  $\text{loop\_j}$  ( $s_{\text{max}}$  is already under  $\text{loop\_j}$ ).
- (b) Step 2: loop transformation. Naive loop fusion fuses  $s_{\text{sum}}$  and  $s_{\text{max}}$  under  $\text{loop\_j}$  ( $s_{\text{max}}$  is already under  $\text{loop\_j}$ ).
- (c) Step 3: pattern matching on the compute statement of  $L_t = s_{\text{sum}}$ .

$$y = g(x, c) = \exp(c - x) \Rightarrow c = g_c^{-1}(x, y) = x + \ln(y)$$

$$h(t, r, r') = g(r', r + \ln(t)) = \exp(r - r') \cdot t$$

Proving commutativity with  $f$ :

$$h(x + y, r, r') = \exp(r - r') \cdot (x + y) = h(x, r, r') + h(y, r, r')$$

- (d) Step 4: finding the repair function  $h$ . Find the inverse of  $g$ , use Equation 6 to find  $h$ , and prove Equation 5 (commutativity with  $f$ ) for  $h$ .

$$X_t[\phi_t(i)] = [X_t[\phi_t(i)] \circ (f)] \circ g(X_r[\phi_r(i)], C[\phi_c(i)])$$

$$xsum[i] = xsum[i] + \exp(input[i, j] - xmax[i])$$

$$X_t = xsum; \quad X_r = xmax; \quad C = inp$$

$$f = +; \quad g(x, c) = \exp(c - x)$$

For  $s_{\text{max}}$ , cache its output  $xmax$  for the previous iteration:

$$xmax\_0[i] := xmax[i]^{(j-1)}; \quad xmax\_1[i] := xmax[i]^{(j)}$$

Apply  $h(t, r, r')$  with  $r = xmax\_0[i]$  and  $r' = xmax\_1[i]$ :

$$xsum[i] = \exp(xmax\_0[i] - xmax\_1[i]) \cdot xsum[i]$$

$$+ \exp(inp[i, j] - xmax\_1[i])$$

(e) Step 5: applying the repair function.

**Figure 10.** All intermediate results of rolling update, when applied to Figure 1a.

### C.2 Privatization

Figure 11 presents privatization combined with rolling update in Neptune. On top of the rolling update output in Figure 1c, we privatize  $s_{\text{max}}$  and  $s_{\text{sum}}$  with a split size of 2.  $xmax\_1p$  and  $xsump$  are the local arrays.

```

1  for i in range(2):
2      xmax_0[i] = -inf
3      for j1 in range(2):
4          for j2 in range(2):
5              # max_local
6              xmax_1p[i, j1] = max(xmax_1p[i, j1], inp[i, j1 * 2 + j2])
7              # max_global
8              xmax_1[i] = max(xmax_1[i], xmax_1p[i, j1])
9              for j2 in range(2):
10                 # sum_local
11                 xsump[i, j1] += exp(inp[i, j1 * 2 + j2] - xmax_1[i])
12                 xsum[i] = exp(xmax_0[i] - xmax_1[i]) * xsum[i] + xsump[i, j1]
13                 xmax_0[i] = xmax_1[i]

```

**Figure 11.** Privatization combined with rolling update in Neptune.

## D Proofs of Rolling Update Correctness Theorems

We use these abbreviations for the following proofs:

$$\begin{aligned} C[\phi_c(i,j)] &=: C_j; & X_t[\phi_t(i)]^{(j)} &=: X_t^{(j)}; \\ X_r[\phi_r(i)]^{(\text{next}(j))} &=: X_r^{(\text{next}(j))} & X_r[\phi_r(i)]^{(j)} &=: X_r^{(j)}; \end{aligned}$$

because all the proofs involve a single loop nest, where the map iteration vector  $i$  is unambiguous.

*Proof of Theorem 4.2.* We assume that  $h$  satisfies the conditions of Eqns. 4 and 5, and prove that  $h$  meets the definition 4.1 which is an equality. The left-hand side of the equality is  $h$  applied to the reduce expression

$$\mathcal{R}\left(f, 0 \preceq j' \preceq j_0, g(X_r^{(j)}, C_{j'})\right) =: R_{j_0}^{(j)}$$

and the right-hand is the updated reduce expression

$$\mathcal{R}\left(f, 0 \preceq j' \preceq j_0, g(X_r^{(\text{next}(j))}, C_{j'})\right) =: R_{j_0}^{(\text{next}(j))}$$

We use  $j_0$  as the reduce range to distinguish it from the tag  $j$ . We prove by induction over the reduce range  $j_0$ :

$$h\left(R_{j_0}^{(j)}, X_r^{(j)}, X_r^{(\text{next}(j))}\right) = R_{j_0}^{(\text{next}(j))} \quad (10)$$

for  $j_0$  from 0 to  $j$ , while all the tags are fixed.

- Base case: when  $j_0 = 0$ ,  $R_{j_0}^{(j)}$  and  $R_{j_0}^{(\text{next}(j))}$  are each a single term,

$$R_0^{(j)} = g(X_r^{(j)}, C_0); \quad R_0^{(\text{next}(j))} = g(X_r^{(\text{next}(j))}, C_0)$$

so the condition to prove simplifies to

$$h\left(g(X_r^{(j)}, C_0), X_r^{(j)}, X_r^{(\text{next}(j))}\right) = g(X_r^{(\text{next}(j))}, C_0)$$

which is true by applying Eqn. 4.

- Inductive step: for any  $j_0$  where the inductive hypothesis Eqn. 10 is true, we add one term to  $R_{j_0}^{(j)}$ :

$$R_{\text{next}(j_0)}^{(j)} = R_{j_0}^{(j)} \bigcircledcirc g(X_r^{(j)}, C_{\text{next}(j_0)})$$

Apply  $h$  to both sides, apply Eqn. 5, then apply Eqn. 4, and finally apply the inductive hypothesis on the underlined term, to get

$$\begin{aligned} & h\left(R_{\text{next}(j_0)}^{(j)}, X_r^{(j)}, X_r^{(\text{next}(j))}\right) \\ &= h\left(R_{j_0}^{(j)} \bigcircledcirc g(X_r^{(j)}, C_{\text{next}(j_0)}), X_r^{(j)}, X_r^{(\text{next}(j))}\right) \\ &= h\left(R_{j_0}^{(j)}, X_r^{(j)}, X_r^{(\text{next}(j))}\right) \bigcircledcirc h\left(g(X_r^{(j)}, C_{\text{next}(j_0)}), X_r^{(j)}, X_r^{(\text{next}(j))}\right) \\ &= h\left(R_{j_0}^{(j)}, X_r^{(j)}, X_r^{(\text{next}(j))}\right) \bigcircledcirc g(X_r^{(\text{next}(j))}, C_{\text{next}(j_0)}) \\ &= \underline{R_{j_0}^{(\text{next}(j))} \bigcircledcirc g(X_r^{(j)}, C_{\text{next}(j_0)})} \\ &= R_{\text{next}(j_0)}^{(\text{next}(j))} \end{aligned}$$

Therefore, the inductive hypothesis is true for  $\text{next}(j_0)$ .

By induction, the theorem is true for all  $j_0 \preceq j$ . We substitute  $j_0 = j$  to get

$$h\left(R_j^{(j)}, X_r^{(j)}, X_r^{(\text{next}(j))}\right) = R_j^{(\text{next}(j))}$$

which is the theorem to prove.  $\square$

*Proof of Theorem 4.3.* We prove that Eqn. 6 is a solution to Equation 4 by simple substitution. Since  $g_c^{-1}$  is the second-argument inverse of  $g$ , we have

$$g_c^{-1}(x, g(x, c)) = c$$

In Eqn. 6, substitute  $t = g(r, c)$  to get

$$h(g(r, c), r, r') = g(r', g_c^{-1}(r, g(r, c))) = g(r', c)$$

which is Eqn. 4.  $\square$

*Proof of Theorem 4.4.* The proof is that the recurrent form in Eqn. 7 (with tag added for clarity)

$$X_t^{(j)} = h(X_t^{\text{prev}(j)}, X_r^{\text{prev}(j)}, X_r^{(j)}) \text{ (f)} g(X_r^{(j)}, C_j)$$

is equivalent to the explicit form in Eqn. 3

$$X_t^{(j)} = \mathcal{R}(f, 0 \preceq j' \preceq j, g(X_r^{(j)}, C_{j'})) =: R_j^{(j)}$$

i.e.,  $X_t^{(j)} = R_j^{(j)}$  for all  $j$  in the iteration domain. We prove it by induction on  $j$ .

- Base case: when  $j=0$ , the recurrent  $X_0$  has iterated once:

$$X_t^{(0)} = g(X_r^{(0)}, C_0)$$

and the explicit  $X_t^{(0)}$  has a single term:

$$R_0^{(0)} = g(X_r^{(0)}, C_0)$$

and they are equal, so the inductive hypothesis is true.

- Inductive step: for any  $j$  where the inductive hypothesis is true, the next iteration  $\text{next}(j)$  updates the recurrent  $X_t$  once. We write down the updated value, apply the inductive hypothesis to convert to explicit form, then use the tag-updating property of  $h$  to get

$$\begin{aligned} & X_t^{\text{next}(j)} \\ &= h(X_t^{(j)}, X_r^{(j)}, X_r^{\text{next}(j)}) \text{ (f)} g(X_r^{\text{next}(j)}, C_{\text{next}(j)}) \\ &= h(R_j^{(j)}, X_r^{(j)}, X_r^{\text{next}(j)}) \text{ (f)} g(X_r^{\text{next}(j)}, C_{\text{next}(j)}) \\ &= R_j^{\text{next}(j)} \text{ (f)} g(X_r^{\text{next}(j)}, C_{\text{next}(j)}) \\ &= R_{\text{next}(j)}^{\text{next}(j)} \end{aligned}$$

Therefore, the inductive hypothesis is true for  $\text{next}(j)$ .

By induction, the theorem is true for all  $j \in \mathcal{D}^s$ . □

```

stmt := loop | store | seq_stmt
seq_stmt := stmt stmt+
loop := [ann] for id in range(expr): stmt
| for id+ in grid(expr+): stmt
ann := blockIdx.x | vectorized | ...
store := id[expr*]=expr
expr := lit | id | id[expr*] | op(expr*)
op := + | - | ... | exp | log | ... | select

```

Figure 12. Neptune loop-scalar IR syntax.

## E Neptune IR Syntax and Translation

Figures 12 and 13 show the syntax of Neptune’s loop-scalar IR and tile IR respectively. The loop-scalar IR is where schedule-based optimizations in Neptune happen, and tile IR enables Neptune’s tile optimizer to automate low-level optimizations. Neptune’s loop-to-tile translation bridges these two IRs.

Loop-to-tile translation converts a program in the loop-scalar IR into a program in the tile IR. The translation consists of three steps: AST partitioning, access function relaxation, and dimension order reconciliation. In Section 5, we have described the last step, while demonstrating the first two steps with an example in Figure 4. This section describes how the translation works in more detail. We give a new example of tile IR program in Figure 14, which is the result of tensorizing the program in Figure 11.

Loop-to-tile translation finds subtrees in the input AST that describe computation on tensor tiles, and converts them into tile store statements. This process is called *tensorization*. Non-tensorizable AST nodes are kept in the output program. AST partitioning marks tensorizable subtrees by examining and partitioning each loop nest. Access function relaxation applies to the inner part of a partitioned loop nest. It converts each array access into a tile access and discards the inner loops. Dimension order reconciliation checks the dimension order of each tile access and changes them when necessary.

```

1 for i in range(2):
2     xmax_0[i] = -inf
3     for j1 in range(2):
4         xmax_1p[i, j1] = reduce(
5             max, inputs[i, j1*2 : j1*2+2], dim=1)
6         xmax_1[i] = max(xmax_1[i], xmax_1p[i, j1])
7         xsump[i, j1] = reduce(+, dim=1,
8             exp(inputs[i, j1*2 : j1*2+2] - xmax_1[i]))
9         xsum[i] = (
10             exp(xmax_0[i] - xmax_1[i])
11             * xsum[i] + xsump[i, j1]
12         )
13     xmax_0[i] = xmax_1[i]

```

Figure 14. The result of tensorizing the program in Figure 11.

```

stmt := loop | storet | stmt*
idx := expr | expr:expr | None
storet := id[idx*]=exprt
exprt := id[idx*] | op(exprt*)
| reduce(op, exprt, dim=i)
| permute(exprt, order=(i*))

```

Figure 13. Neptune tile IR syntax. Non-terminals that are the same as Figure 12 are omitted.

**AST Partitioning.** AST partitioning selects subtrees on the input AST that do not include sequential statements (*seq\_stmt* in Figure 12) and annotated parallel loops (e.g. `blockIdx.x i in range(32)`). Sequential statements and loop annotations do not have a counterpart in tile expressions, so they are excluded from tensorization.

Partitioning works bottom-up from store statements. A store statement *s* is a leaf statement in the loop-scalar IR and has loop parents  $\mathbf{i} := (i_1, \dots, i_K)$  from the root of the AST. For each *s*, partitioning finds the outermost loop  $i_p \in \mathbf{i}$  such that the whole subtree  $i_p$  is structurally tensorizable. We denote this partitioned AST around *s* as  $part(\mathbf{i}_o : \mathbf{n}_o, \mathbf{i}_i : \mathbf{n}_i)\{s\}$ , where  $\mathbf{i}_o := (i_1, \dots, i_{p-1})$  and  $\mathbf{i}_i := (i_p, \dots, i_K)$ . The statement *s* and inner loops  $\mathbf{i}_i$  form a perfect loop nest  $nest(\mathbf{i}_i : \mathbf{n}_i)\{s\}$ . In the input program Figure 11, since the body of the loop  $j_1$  is a sequential statement, partitioning stops at  $j_1$  and returns  $part((i, j_1) : (2, 2), (j_2) : (2))$  for stores `max_local` and `sum_local`. The partitions of other stores have empty inner loops.

**Access Function Relaxation.** For each AST partition  $part(\mathbf{i}_o, \mathbf{n}_o, \mathbf{i}_i, \mathbf{n}_i)\{s\}$ , access function relaxation converts each array access of *s* into a tile access (producing *s'*), such that the region *s* accesses in  $\mathbf{n}_i$  iterations is the same as the region accessed by *s'* in one iteration. We assume that *s* has the following form:

$$X_0[\phi_0(\mathbf{i}_o, \mathbf{i}_i)] = F(X_1[\phi_1(\mathbf{i}_o, \mathbf{i}_i)], \dots, X_K[\phi_K(\mathbf{i}_o, \mathbf{i}_i)]) \quad (11)$$

Relaxation finds the range of each  $\phi_k$  over the inner iteration domain  $\mathbf{n}_i$ , and checks if this range is a tile that fits in the tile syntax of the IR. We now define these notions precisely.

Let  $\phi(\mathbf{i}_1, \mathbf{i}_2)$  be an affine access function

$$\phi: \mathcal{D}_1 \times \mathcal{D}_2 \rightarrow \mathbb{Z}^M \quad \phi(\mathbf{i}_1, \mathbf{i}_2) = U\mathbf{i}_1 + V\mathbf{i}_2 + b$$

where  $\mathcal{D}_1 \subset \mathbb{Z}^{N_1}$ ,  $\mathcal{D}_2 \subset \mathbb{Z}^{N_2}$ ,  $U \in \mathbb{Z}^{M \times N_1}$ ,  $V \in \mathbb{Z}^{M \times N_2}$ , and  $b \in \mathbb{Z}^M$ . For a fixed  $\mathbf{i}_1 \in \mathcal{D}_1$ , the set of values  $\phi(\mathbf{i}_1, \mathbf{i}_2)$  can take while varying  $\mathbf{i}_2 \in \mathcal{D}_2$  is the image of  $\phi$  at  $\mathbf{i}_1$ :

$$Im_{\phi, i_0}(\mathbf{i}_1) = \{\phi(\mathbf{i}_1, \mathbf{i}_2) : \mathbf{i}_2 \in \mathcal{D}_2\}$$

Relaxation finds  $Im_{\phi, i_0}(\mathbf{i}_0)$  and requires it to be a tile so that it can be expressed in the tile IR. Since  $\phi$  is affine and the domain of  $\mathbf{i}_i$  is a box,  $Im_{\phi, i_0}(\mathbf{i}_0)$  is a zonotope for all  $\mathbf{i}_o$ , which are more general than tiles (axis-aligned boxes). We place a constraint

on  $V$  to ensure that  $\text{Im}_{\phi, i_i}(\mathbf{i}_o)$  is a tile: each column of  $V$  has at most one non-zero entry. We refer to this constraint as  $V$  being *1-sparse*. For example, in Figure 11, the statement `max_local` has an array access `inp[i, j1 * 2 + j2]`. Its access function is

$$\phi((i, j_0), (j_1)) = \begin{pmatrix} 1 & 0 \\ 0 & 2 \end{pmatrix} (i, j_0)^T + \begin{pmatrix} 0 \\ 2 \end{pmatrix} (j_1)^T$$

so  $V$  is 1-sparse. If  $V$  is not 1-sparse, tensorization shrinks  $\mathbf{i}_i$  by moving loops from  $\mathbf{i}_i$  to  $\mathbf{i}_o$ , which removes rows from the top of  $V$ , until  $V$  is 1-sparse.

If  $\text{Im}_{\phi, i_i}(\mathbf{i}_o)$  produces a tile, we use the notation  $\Phi(\mathbf{i}_o)$  instead to express that it is a valid *tile access function*. Relaxation rewrites each  $X_k[\phi_k(\mathbf{i}_o, \mathbf{i}_i)]$  in Equation 11 into a tile access  $X_k[\Phi_k(\mathbf{i}_o)]$ , producing

$$X_0[\Phi_0(\mathbf{i}_o)] = F(X_1[\Phi_1(\mathbf{i}_o)], \dots, X_K[\Phi_K(\mathbf{i}_o)]) \quad (12)$$

**Dimension Order Reconciliation.** Dimension order reconciliation has been described in Section 5. It works on an *einops* [32] expression such as `c r -> r c`, which we can derive from the output of the last step (Equation 12 and the  $V$  matrix of access functions). Since  $V$  is 1-sparse, every non-zero column of  $V$  is a multiple of a standard basis vector:

$$\begin{aligned} \forall j \in \{1, \dots, |\mathbf{i}_i|\} \text{ s.t. } V_{\cdot j} \neq 0 \\ \exists i(j) \in \{1, \dots, M\}, \lambda_j \in \mathbb{Z}, \quad V_{\cdot j} = \lambda_j \vec{e}_{i(j)} \end{aligned}$$

The mapping  $i(j)$  relates a column of  $V$  (corresponds to a loop in  $\mathbf{i}_i$ ) to a standard basis vector (corresponds to a dimension in the tile). We use this mapping to find a dimension order for each access function  $\Phi_i$  in Equation 12, and assemble them into an *einops* expression.

## F Additional Evaluation

### F.1 Compilation Statistics

We provide some statistics Neptune's compilation pipeline when generating kernels we have evaluated in Section 8. For these evaluated operators, Neptune with 128 autotuning iterations takes 1.5 to 10 minutes to run on each setup. Triton-based tile optimization takes 50% to 90% of the time (depending on the input shape). Neptune's template-guided optimization (rolling/split-k update) takes 5% to 10% of the time (does not depend on input shape), and the rest is TVM autotuning search algorithm.

### F.2 Operator Evaluation

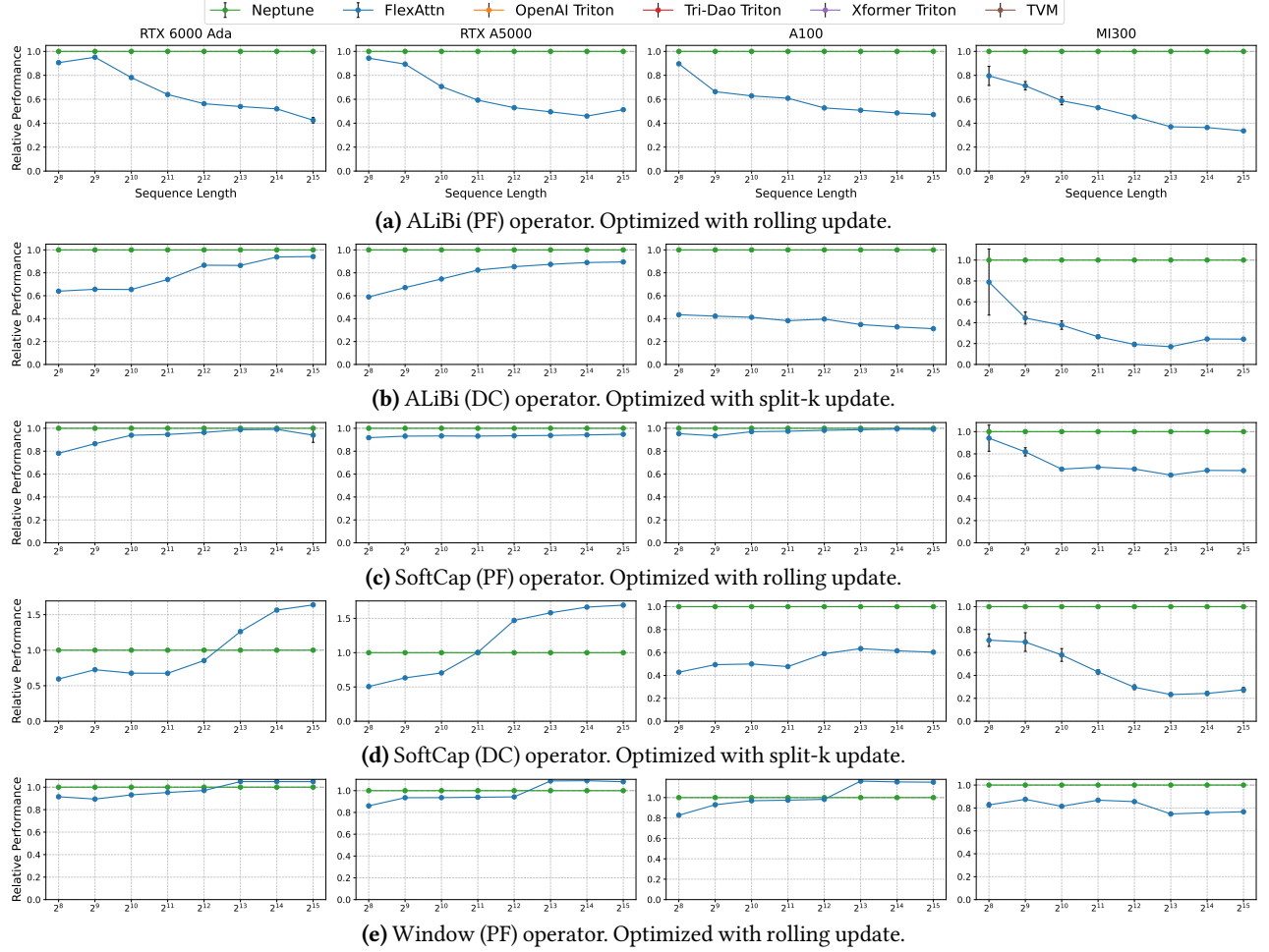


**Figure 15.** Performance of Neptune vs. other tensor compilers on the five operators not shown in Figure 5.

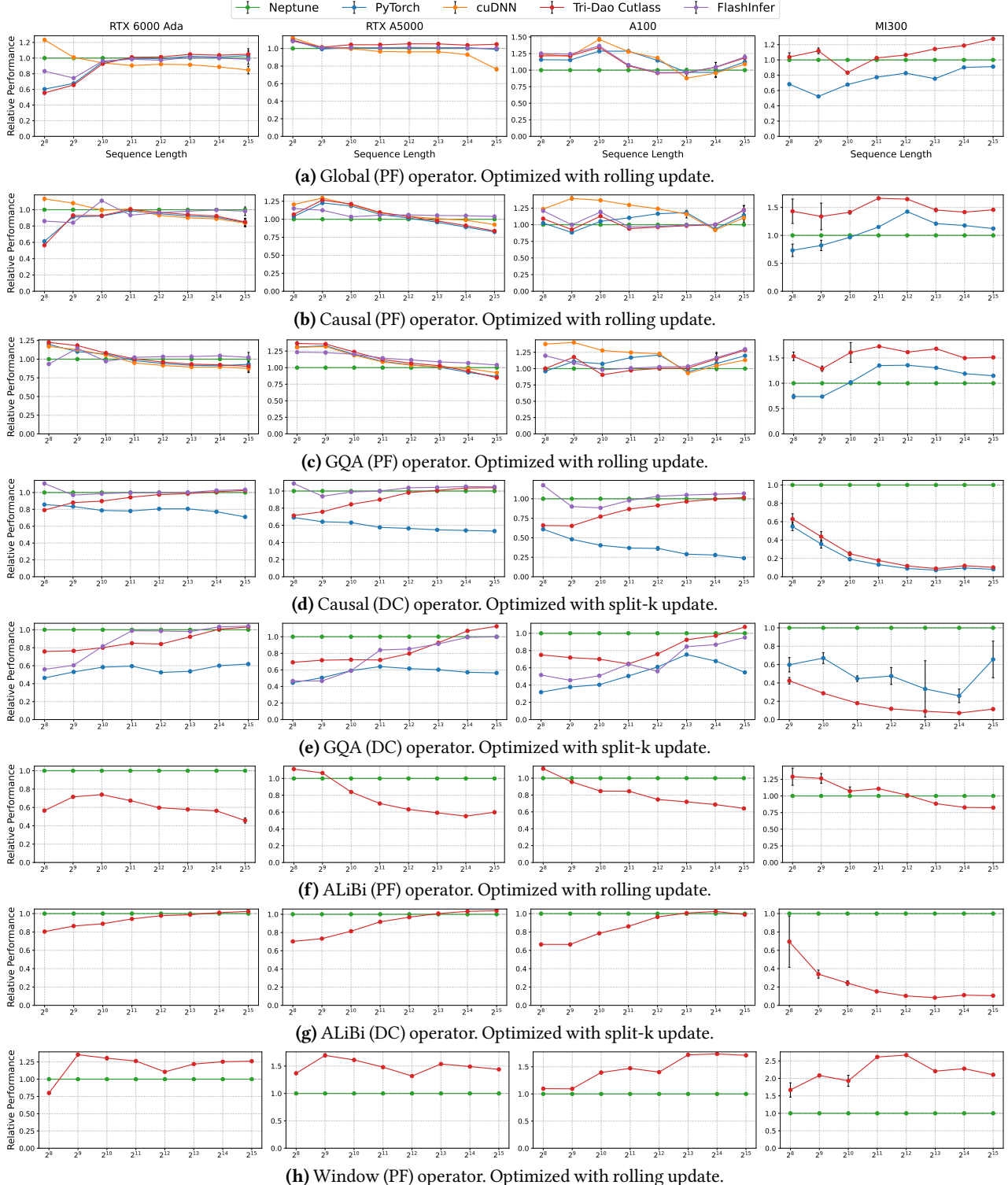


**Figure 16.** Performance of Neptune vs. tensor libraries on 8 operators for which library baselines exist (we were unable to find the library implementations of SoftCap PF/DC).

### F.3 Scalability Test

Figure 17 extends the scalability test of Figure 6 to all the 10 operators, 4 GPUs and all implementations used in our Evaluation section. We still use a sequence length of 8192 and batch sizes up to 32.

Figures 17a to 17f shows that the throughput of all prefill kernels decrease as input batch size increases. By closely inspecting profiling results, we find that larger workloads are more likely to trigger GPUs' clock throttling. Figure 18 shows a profile in the Nvidia Nsight System profiler, with a kernel (flash\_fwd\_kernel) that runs for 281 milliseconds. The GPU compute clock ("GPC Clock Frequency") starts to throttle within 50 milliseconds after the kernel starts.

In Figures 17g to 17j, the decoding kernels exhibit the opposite trend: throughput increases with batch size. Decoding kernels are much less compute-bound than prefill kernels to trigger clock throttling, and benefit from increasing parallelism at larger batch sizes.

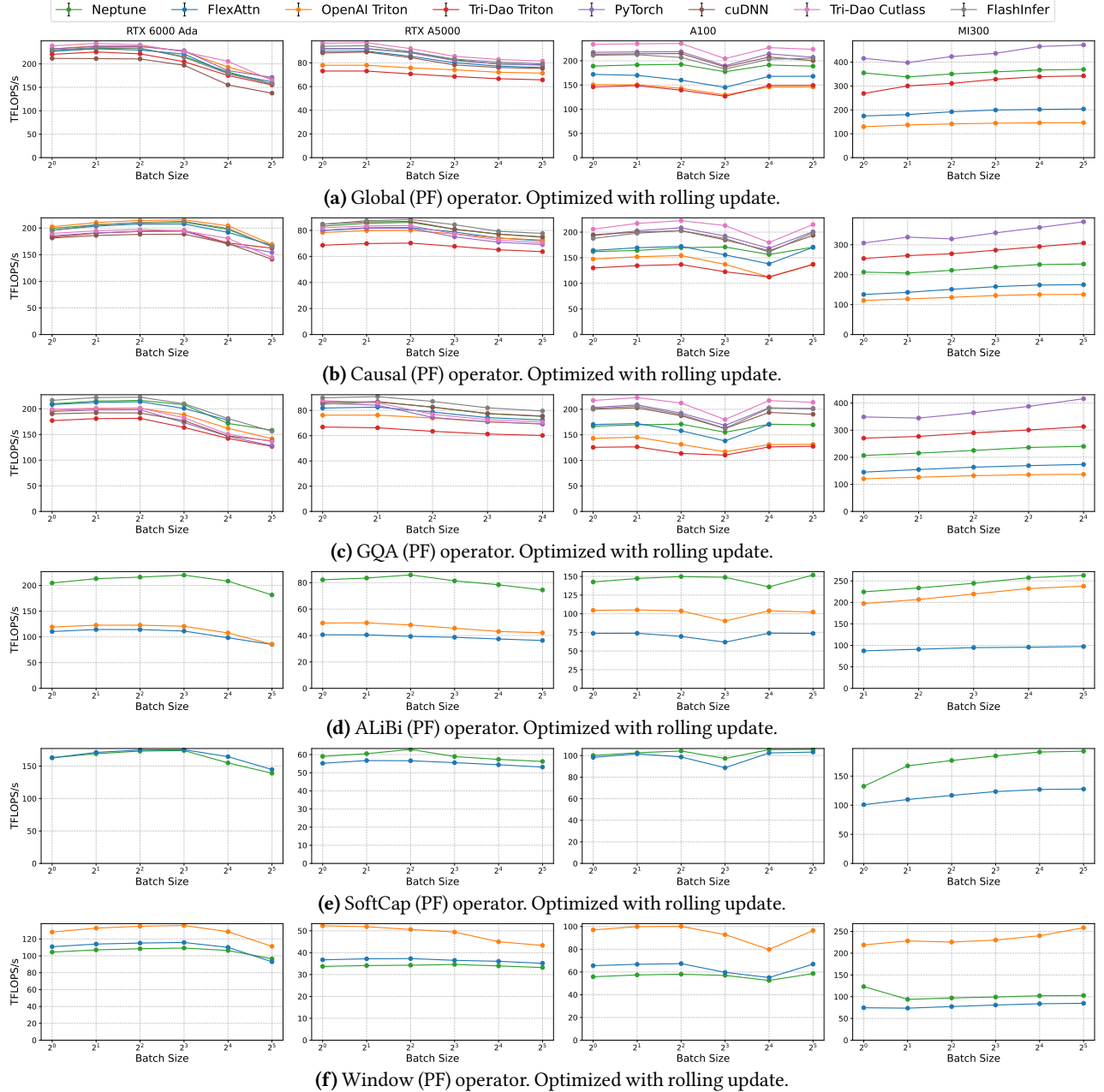
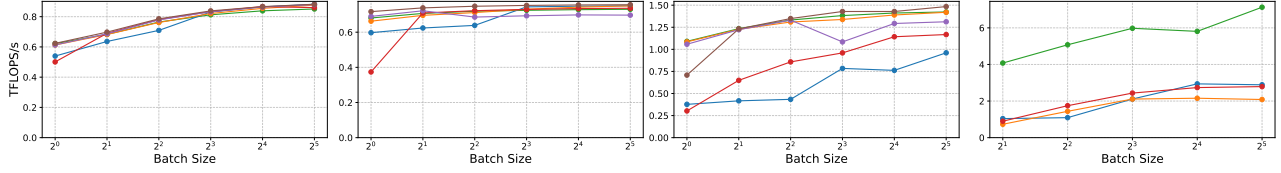
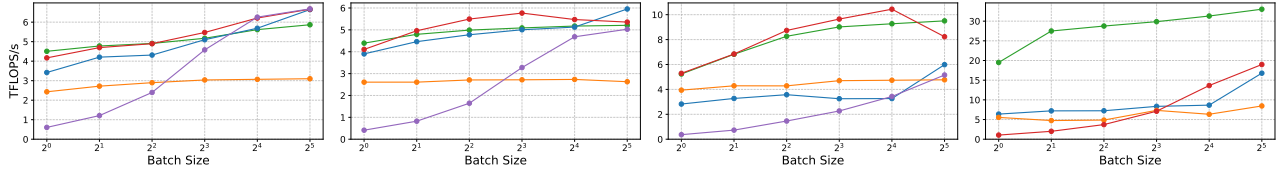


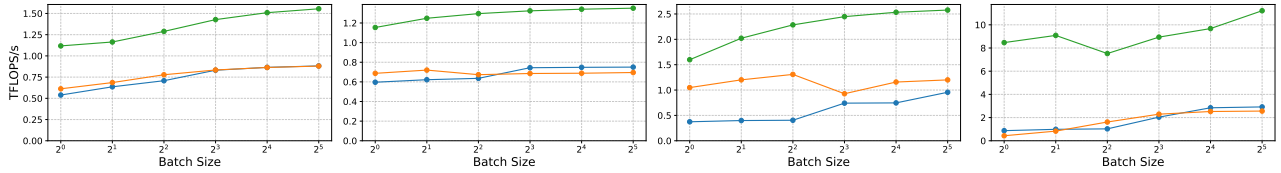
**Figure 17.** Throughput of Neptune kernels and multiple baselines over increasing batch size, for all 10 operators on all 4 GPUs. The y-axis shows throughput in TFLOPS/sec, and the x-axis shows batch size.



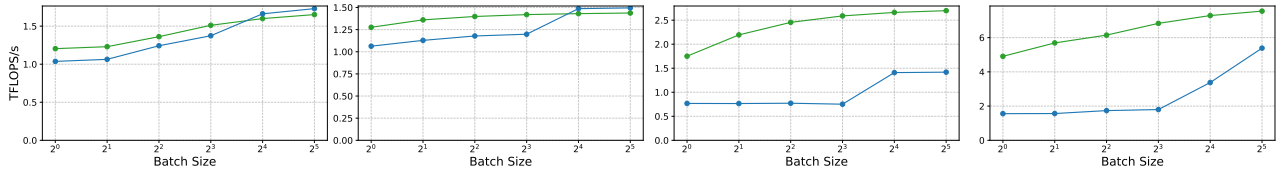
(g) Causal (DC) operator. Optimized with split-k update.



(h) GQA (DC) operator. Optimized with split-k update.



(i) ALiBi (DC) operator. Optimized with split-k update.



(j) SoftCap (DC) operator. Optimized with split-k update.

**Figure 17.** (Continued) Throughput of Neptune kernels and multiple base- lines over increasing batch size, for all 10 operators on all 4 GPUs. The y-axis shows throughput in TFLOPS/sec, and the x-axis shows batch size.

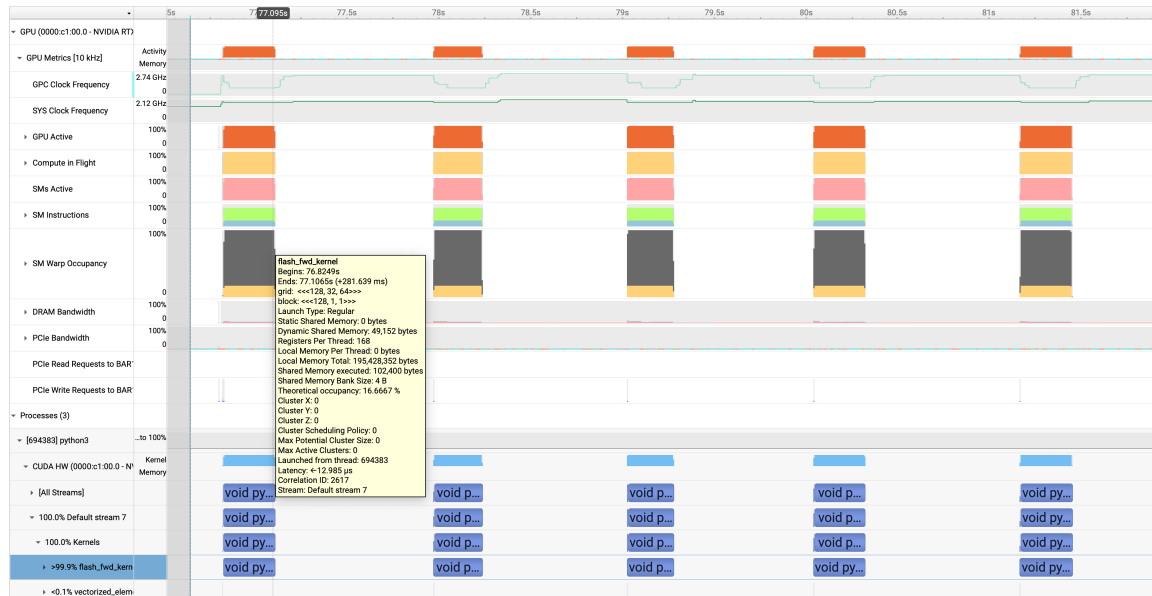


**Figure 18.** Timeline view of a profile in the Nvidia Nsight System profiler. The bottom rows show when the kernels are executing, and the “GPC Clock Frequency” row near the top shows the frequency of the GPU graphic clock over time.